COMPUTATIONAL AND EXPERIMENTAL INSIGHT INTO SINGLE-MOLECULE

PIEZOELECTRIC MATERIALS

by

Christopher Wayne Marvin

Bachelors of Science in Chemistry, College of Charleston, 2011

Submitted to the Graduate Faculty of the

Kenneth P. Dietrich School of Arts and Sciences in partial fulfillment

of the requirements for the degree of

Doctor of Philosophy

University of Pittsburgh

2017

UNIVERSITY OF PITTSBURGH

DIETRICH SCHOOL OF ARTS AND SCIENCES

This dissertation was presented

by

Christopher Wayne Marvin

It was defended on

March 21st, 2017

and approved by

Seth Horne, Associate Professor, Chemistry Department

Haitao Liu, Assisstant Professor, Chemistry Department

William Clark, Professor, Department of Mechanical Engineering & Materials Science

Dissertation Advisor: Geoffrey Hutchison, PhD, Associate Professor, Chemistry Department

COMPUTATIONAL AND EXPERIMENTAL INSIGHT INTO SINGLE-MOLECULE

PIEZOELECTRIC MATERIALS

Christopher Wayne Marvin, PhD

University of Pittsburgh, 2017

Piezoelectric materials allow for the harvesting of ambient waste energy from the environment. Producing lightweight, highly responsive materials is a challenge for this type of material, requiring polymer, foam, or bio-inspired materials. In this dissertation, I explore the origin of the piezoelectric effect in single molecules through density functional theory (DFT), analyze the piezoresponse of bio-inspired peptidic materials through the use of atomic and piezoresponse force microscopy (AFM and PFM), and develop a novel class of materials combining flexible polyurethane foams and non-piezoelectric, polar dopants. For the DFT calculations, functional group, regiochemical, and heteroatom derivatives of [6]helicene were examined for their influence on the piezoelectric response. An aza[6]helicene derivative was found to have a piezoelectric response (108 pm/V) comparable to ceramics such as lead zirconium titanate (200+ pm/V). These computed materials have the possibility to compete with current field-leading piezomaterials such as lead zirconium titanate (PZT), zinc oxide (ZnO), and polyvinylidene difluoride (PVDF) and its derivatives.

The use of AFM/PFM allows for the demonstration of the piezoelectric effect of the self-assembled monolayer (SAM) peptidic systems. Through PFM, the influence that the helicity and sequence of the peptide has on the overall response of the molecule can be analyzed. Finally, development of a novel class of piezoelectrics, the foam-based materials, expands the current understanding of the qualities required for a piezoelectric material from ceramic and rigid materials to more flexible, organic materials. Through the exploration of these novel types of piezoelectric materials, new design rules and figures of merit have been developed.

TABLE OF CONTENTS

LIST OF TABLES

LIST OF FIGURES

Appendix Figures

ACKNOWLEDGEMENTS

computational, experimental, and analytical chemistry. Dr. Liu, Dr. Horne, and Dr. Clark, my thanks go to you for your time, questions, and suggestions regarding my growth as a Ph.D. chemist. I want to thank you, Dr. Hutchison, for everything you have helped with me over the last few years, from research questions, to off-topic discussions about everything else.

Lastly, I would like to thank my family and friends. My mom and dad have been supportive the whole time, joking about me becoming a "lifetime student." I love you for the advice and help that you have given me in support of my life and career choices. My brothers and their families, I want to thank you for giving me the great times that we had as children. To my second family, the Smiths, you have taken me in as one of your own and made me feel comfortable after moving here all on my own. Thank you for everything you have done and for becoming my second family. Matt, Brendan, and my other friends, thank you for the amazing times that we had at the game store and the trip down to Richmond; "Welcome to the South, boys."

Lastly, to those who I have failed to mention, thank you for being the guardian angels that you are, whether you realize it or not, you have affected and helped me achieve this lifelong goal of mine. I know that through the help you provided, I can do anything I set my mind to.

1.0   INTRODUCTION

1.1   ENERGY HARVESTING

Energy harvesting is a critical goal to address energy efficiency and modern energy demands. There is a demand for materials to harvest the ambient vibrations from the environment and can be applied to different surfaces to convert energy such as body,[1] pipe walls for fluid flow,[2] and portable devices.[3] Having the ability to extend the battery lifetime of portable electronics through ambient vibrations such as the wind and human motion is a desired characteristic of these energy harvesting materials. These devices can harvest the energy from walking around with the device in your pocket or the waste energy from walking around a building can be used to supplement the power requirements of the building. Through this effect, piezoelectric materials have been used in a wide variety of applications ranging from actuators,[4] sensors and biosensors,[5,6] motors,[7,8] and energy harvesters.[9,10]

1.2   PIEZOELECTRIC ENERGY HARVESTING MATERIALS

Piezoelectric materials can be utilized in micro- and nano-power generators because of their ability to harvest ambient vibrational energy. Lead zirconium titanate (PZT) has been utilized in a micro energy harvesting device with a power output of 1.4 µW and 1.6 V at a

frequency of 870 Hz.[11] This type of device is useful for harvesting waste vibrations from machinery due to their frequency of vibrations being around 100 Hz, however, a large amount of work is still needed to match the optimal harvesting frequency with the working frequency. A piezoelectric nanogenerator based on aligned ZnO nanowires grown on a solid substrate and is an excellent alternative to PZT due to the lack of lead in the material, making it an environmentally green material. These ZnO materials have a power generation of 0.5 pW, however, the mass of ZnO is significantly lower than PZT, leading to lightweight devices. However, the resonance frequency of the ZnO materials is ~10 MHz, which is much higher than conventional circumstances providing room for optimization.[12]

1.3   CONVENTIONAL PIEZOELECTRICS.

Conventional piezoelectric materials include ceramics (lead zirconium titanate, PZT),[13] nanowires/nanorods (zinc oxide, ZnO),[14] and polymers (polyvinylidene difluoride, PVDF).[15] The application of mechanical stress to the material causes a polarization to occur in the material; This induced polarization is called the direct piezoelectric effect. The interconversion can be either direct, converting force into charge, or converse, converting electric charge into stress. Conversely, if an electric field is applied to a piezoelectric material, the unit cell will deform. The total response of the piezoelectric material requires alignment of the dipole moments of the individual unit cells. These dipoles can be aligned through the application of an external electric field while the material is above the Curie temperature, T_C, in a process called poling. The larger the percentage of overall dipoles that are aligned, the larger the piezoelectric response of the bulk material.[16]

1.3.1   Origin of the piezoelectric property.

The piezoelectric property is exhibited when a material has a non-centrosymmetric unit cell.[17] For inorganic and ceramic piezoelectric materials, 20 of the 32 crystal classes exhibit direct piezoelectricity,[18] including both polar and non-polar crystals. For a non-polar crystal, this effect can occur when a deformation causes an induced polarization to occur, as in ZnO nanowires.[19] Perovskite piezoelectric materials require a high voltage to be applied to the material, a process called poling, in order to produce the necessary non-centrosymmetric unit cell. Poling of a perovskite piezoelectric is required since the unit cell is centrosymmetric otherwise. Poling breaks the centrosymmetry by forcing the central Zr^{4+} or Ti^{4+} out and into half of the unit cell, creating a dipole moment. Ceramic PZT and ZnO nanowires, Figure 1.1, are two common examples of inorganic piezoelectric structures. Conventional piezoelectric materials come in a variety of classes: non-centrosymmetric inorganic crystals/ceramics such as lead zirconium titanate (PZT),[20] zinc oxide nanowires/nanorods (ZnO),[21] and quartz;[22] organic polymers such as polyvinylidene difluoride and its copolymers;[23] and 2D nanomaterials such as MoS_2.[24]
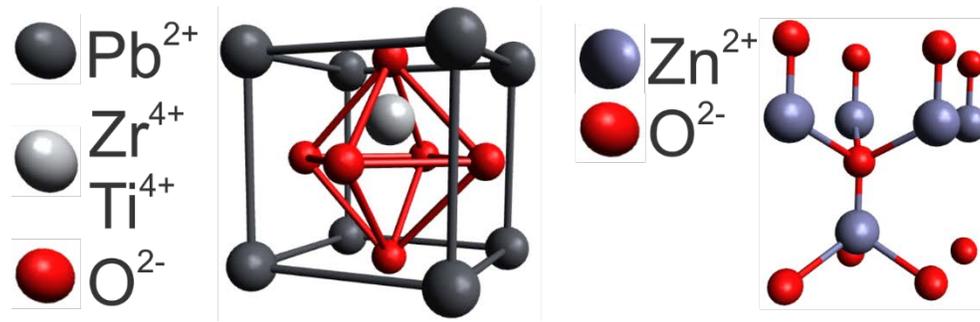
Figure 1.1. Repeat units for the unit cells of: left.) Lead zirconium titanate perovskite and right.) ZnO Wurzite cell.

1.3.2 Piezoelectric coefficient

The generated charge and the force applied are directly related by the piezoelectric coefficient, d_{ij}, where i is the direction of the force, and j is the direction of the electric field. The most common piezoelectric coefficient, d_{33}, relates the force and charge in the z-direction. To represent their primary function, the units of d_{33} are pC N^{-1} when referencing the direct effect, since a force is applied and there is a resultant force; and pm V^{-1} for the converse effect, due to the deformation due to the applied bias. These units are equivalent as shown in Equation (1.1) below:

$$\frac{pC}{N} = \frac{pV \times F}{N} = \frac{pV \times J}{N \times V^2} = \frac{pJ}{N \times V} = \frac{pm \times N}{N \times V} = \frac{pm}{V} \tag{1.1}$$

where C is coulombs, N is the force in newtons, V is volts, F is farad, J is joules, and m is meters. A larger deformation or higher charge density or voltage will be created from materials with a larger piezoelectric coefficient.

4

1.4   RATIONAL DESIGN OF NOVEL MATERIALS

The discovery of target molecules with an optimized piezoelectric response can be performed using "virtual synthesis." With computational chemistry, it is possible to screen a wide range of molecules in a shorter amount of time than it would take to synthesize and analyze novel compounds. With this quality, computational design of novel materials saves time, effort, and money spent in the lab on failed or insignificant materials. Possible candidates can be screened for desired properties without spending unnecessary weeks at the benchtop to produce them. While the quantitative accuracy of a method may be unknown, the relative qualitative properties can produce a vast amount of information.

In regards to the piezoelectric effect, agreement between computed and experimental responses is quite high as shown by Werling, *et al.*[25] In this work, the authors computed the piezoelectric coefficient of the hydrogen bond in crystalline methyl-nitroaniline by using density functional theory (DFT)/B3LYP. The high agreement demonstrated therein allows for great confidence in the method applied for the calculations applied to the single molecular piezoelectric systems.

1.5   SELF-ASSEMBLED MONOLAYERS
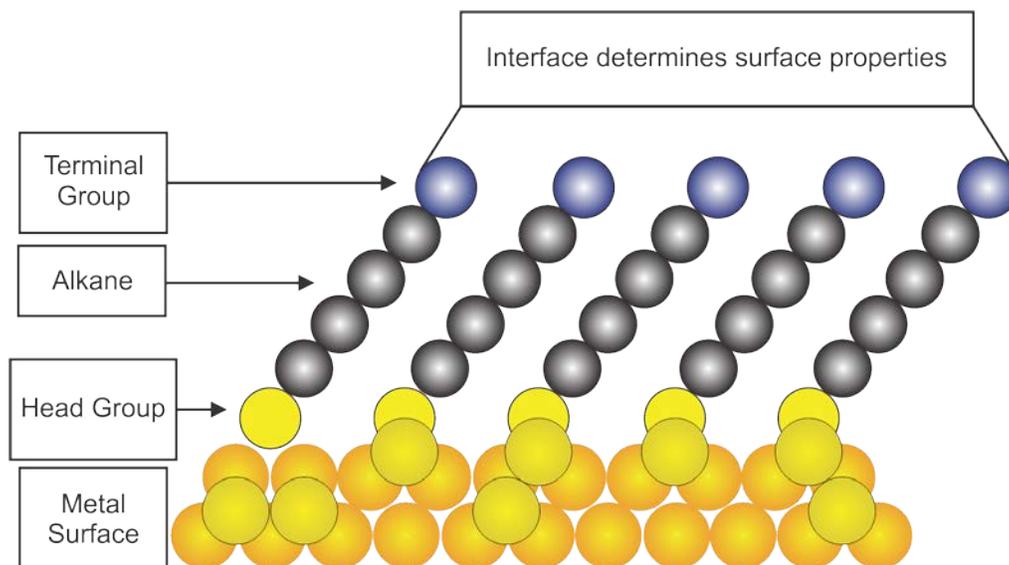
Figure 1.2. Schematic detailing self-assembled monolayer components for alkane-based SAMs.

Organic molecules can be chemisorbed onto a metallic surface in order to form highly-ordered molecular assemblies known as self-assembled monolayers, or SAMs. These monolayers allow for the tailoring of the surface chemistry of the metal surface for preferential characteristics such as hydrophobicity, electronic conductivity, or local optical properties, for example.[26] SAMs are composed of a metallic substrate, an attached head group or ligand, a spacer, and a terminal functional group, as seen in Figure 1.2. SAMs can be formed on many different surfaces between alkanethiols and gold,[27] silver,[28] copper,[28] and other metals.[29,30] Other common substrates include oxides, such as Fe_xO_y, TiO_2, and ITO, and silanes.[26] With these other substrates, a wider range of possible ligands exists including hydroxy-, carboxylic acid-, and amine-terminated molecules. The most common protocol for forming SAMs on these metals is to immerse a freshly cleaned substrate into a dilute (~1-10 mM) ethanolic solution of thiols for 12-

18 h at room temperature.[26] These conditions allow for a high degree of reproducibility across a wide range of alkane thiolates and metal substrates.

Minimization of the free energy of the SAM requires the adoption of high degrees of van der Waals and hydrogen bond interactions with neighboring molecules. Along with this minimized free energy, the SAM molecules acquire up to a 30° angle between the spacer, head group, and substrate for an alkanethiol-based SAM on gold.[26] In the perspective of this dissertation, this angle causes the measured piezoelectric response of the SAM to be less than the computed response since the alignment of the molecules are not directly along the orientation of the applied field.

1.6 PRINCIPLES OF ATOMIC AND PIEZORESPONSE FORCE MICROSCOPY.

The sensitivity of atomic force microscopy (AFM) is ideal for the analysis of SAMs in regards to topography or piezoelectric response. [31] Atomic force microscopy is a form of scanning probe microscopy with a surface resolution on the order of less than a nanometer. This instrument senses the surface of a sample through attraction or repulsion of the surface being analyzed. Using a photodiode, an IR-laser is reflected off a cantilever and measured as the tip interacts with the surface as shown in Figure 1.3. Force measurements, imaging, and surface manipulation can all be measured by AFM techniques. For example, upon calibration of the instrument, the forces between the probe and sample can be determined and used to perform force spectroscopy, such as piezoresponse force microscopy (PFM). An example is that the

topography of a sample can be scanned in three dimensions from the interaction between the tip and the surface creating a height profile of an area of a sample. Manipulation of a sample can be performed by changing the properties of the surface through direct interactions between the probe and the sample, i.e. scanning probe lithography. AFM can be performed in either non-contact or contact mode. The cantilever performs a tapping motion to sense the surface in order to interact with the surface during a non-contact scan.
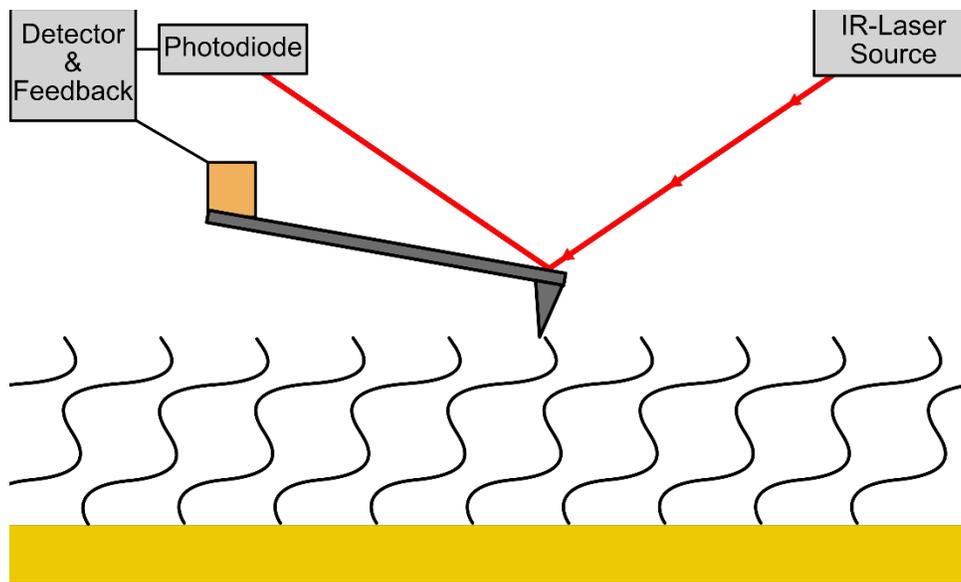
Figure 1.3. Working principle of an atomic force microscope. An IR-laser is placed on a cantilever probe which interacts with the surface of a sample and the IR reflection is measured by a photodiode. Any deformation of this signal is indicative of a change in topography of the surface of the sample.

1.6.1 Piezoresponse force microscopy (PFM).

Piezoresponse force microscopy is a contact-mode AFM technique which utilizes an AC voltage applied to a conductive tip while scanning.[32] The AFM applies an electric voltage and measures changes in the thickness, Δt. This induced Δt of the sample is characteristic of the sample's piezoelectric character. The relationship between the magnitude of the displacement and the applied voltage can be used to calculate the piezoelectric coefficient of the sample. The overall deflection of the cantilever measured by the photodiode in PFM is composed of three distinct parts: the displacement of the tip, the displacement of the sample, and the tip-sample interaction. To accurately measure the piezoresponse, only the displacement of the sample must be considered. Since there are three components to the signal, limitations to obtaining quantitative piezoelectric responses are present. These limitations include nonlocal effects from the tip,[33] background signal interference,[34] electrostatic effects from tip-surface interactions,[31] and potential drop from tip to surface.[31]

1.6.2 Dual AC Resonance Tracking (DART) PFM

Dual AC resonance tracking expands on the piezoresponse force microscopy technique by allowing for the cantilever to be operated at or near the contact resonance frequency in order to take advantage of the tip amplification due to this coupling, allowing for quantitative examination of biological and inorganic surfaces.[35] Compared to conventional PFM which tunes at a single frequency, DART-PFM utilizes a frequency feedback loop between two amplitudes within which the contact resonance peak is located. At these boundary frequencies, the amplitude is measured and it is possible to track changes in the resonance behavior, as seen in Figure 1.4.

Due to this tracking, the signal-to-noise ratio is increased since the contact resonance allows for amplification of the signal. This amplification is directly related to the q-factor of the cantilever, a dimensionless quantity inversely dependent on the cantilever energy dissipation;[35] the larger the q-factor, the greater the amplification. Finally, the use of a simple harmonic oscillator model of the tip allows for the amplification factor to be removed, and the actual response can be calculated.
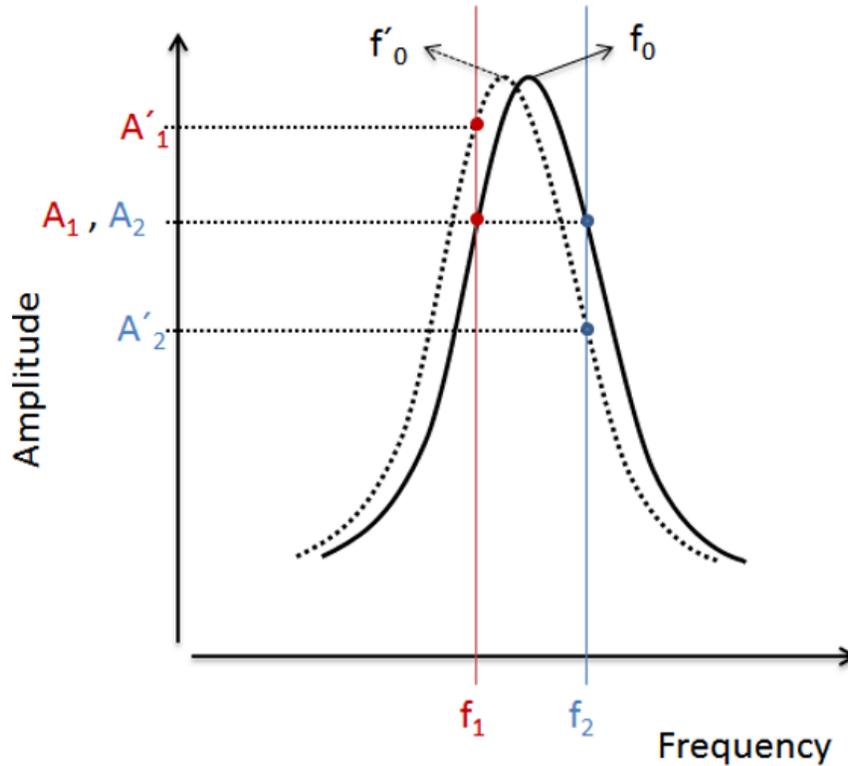
Figure 1.4. Adapted from ref.[35], the working principle of DART-PFM allowing for the frequency tracking technique to be applied.

1.6.3   Potential error in PFM/DART-PFM

There are many possible sources of error that may affect a PFM measurement such as enhancement of the response due to high voltages, unknown tip geometry and thus field shape, tip-sample contact stiffness is finite, and tip-sample electrostatic interactions.[36] Due to the unknown field shape and the finite tip-sample contact stiffness, the calculation of the piezoelectric coefficient will be an underestimate due to the field having a lower impact on the sample than is recorded by the instrument. Another electro-mechanical distortion, electrostriction, can appear during a PFM experiment and can cause an overestimate of the computed piezoelectric response.[37] The difference between electrostriction and piezoelectricity is that electrostriction responds quadratically to an applied electric field, while piezoelectricity is a linear response.

1.7   OVERVIEW AND OBJECTIVES

The objectives of this dissertation are to use the concept of rational design in order to develop novel targets for single-molecule piezoelectric materials with optimized responses using density functional theory (DFT); develop optimized principles for piezoelectric materials with improved response; utilize these design principles to develop piezoelectric peptides with greater responses than other biological materials and demonstrate the response using piezoresponse force microscopy (PFM); and develop a novel class of foam-based piezoelectric materials doped with polar, rigid, small molecules which exhibit very high piezoresponses.

The organization of the thesis is as follows:

Chapter 2 covers the computational and experimental methods utilized in the following chapters. The computational methods utilize density functional theory and multiple applied voltages to compute the piezoelectric response and the experimental methods discuss the use of atomic force and piezoresponse force microscopy to analyze piezoelectricity.

Chapter 3 discusses the computational exploration of single molecule piezoelectric materials based on the [6]helicene and phenanthrene backbone motifs. Density functional theory (DFT) calculations are utilized and the effects of regiochemistry, dipole moment, polarizability, steric interactions, and electron donating and withdrawing character of substituents on the piezoelectric response are analyzed.

Chapter 4 expands the work from chapter 2 to include heteroatom substitutions in the [6]helicene backbone to optimize the piezoelectric response. Still using DFT, it is shown that there is a larger influence on the piezoelectric response from a lack of steric interactions than from the increased (or decreased) electron density of the conjugated ring system by the substitutions made. Nitrogen, oxygen, and sulfur heteroatoms were substituted into various positions in the [6]helicene in order to examine the effects of both electron-rich and electron-poor substitutions.

Chapter 5 demonstrates the experimental analysis of piezoelectric peptide monolayers using piezoresponse force microscopy (PFM) to quantify the piezoelectric response. These peptides differ in degree of helicity as shown by circular dichroism (CD) to assess the impact helicity has on the piezoelectricity.

Chapter 6 discusses the development of a novel class of piezoelectric materials based on the composite of polyurethane foam and rigid, polar, small molecules. This novel material shows

a piezoelectric response on the same order of magnitude of PZT, that is, greater than 200 pC N^{-1}, can be produced from two non-piezoactive components. This chapter demonstrates the relationship between dipole concentration in the composite material and the overall piezoelectric response of the material.

  Chapter 7 concludes the dissertation and provides future directions for the optimization of these flexible peptide- and foam-based piezoelectric materials.

2.0   METHODS

2.1   COMPUTATIONAL METHOD

Gaussian 09[38] and density functional theory (DFT) are used for the computational study of the [6]helicene and phenanthrene piezoelectric molecules in Chapters 3 and 4. The B3LYP functional[39] with the 6-31G(d) basis set are used to optimize all computed structures. DFT is known to be asymptotically incorrect and ignore dispersion,[40-42] thus an example set of calculations were performed on [6]helicene and phenanthrene using B97D,[43] CAM-B3LYP,[44] PBE1PBE,[45] and wB97XD[46] functionals in order to assess any variation in the trends. Since the trends examined in this work appear independent of the functional chosen, B3LYP is selected for the computations for consistency, as no experimental data exists for comparison. High agreement has been found between the experimental piezoelectric coefficient, d_{33}, of 2-methyl-4-nitroaniline, and the computed value using the B3LYP functional.[25]

The molecules are designed in Avogadro[47] in order to obtain a specific frame of reference. This frame of reference is used to align the molecule to consider the geometric deformation in response to an applied external electric field. The direction and magnitude of the electric field are added to the Gaussian input. All final geometries were checked for consistency since local minima exist in regards to certain functional groups (e.g. $-NH_2$ pyramidal inversion). Unless otherwise specified (i.e., for examination of the direct piezoelectric effect), no constraints

are applied to the optimization. Since optimization occurs in the 3N-6 internal degrees of freedom, translations and rotations of the frame of reference can be removed by a select choice of coordinates. We find that even with the automatic selection of internal coordinates from Cartesian coordinates, only small (less than 1-3°) rotations occur.

The piezoelectric coefficient is a tensor derived from the applied electric field and the resulting deformation. In this work, focus is placed on the deformation along the same axis as the electric field, both in the z-direction, described as d_{33}. The z-direction, although potentially arbitrary, is defined to be the approximate lowest energy vibrational breathing mode. The d_{33} coefficient is calculated from the difference between the molecular length at an applied field (l_{max}) and at zero applied field (l_{zero}) using Equation 2.1:

$$d_{33}\left[\frac{pm}{V}\right] = \frac{(l_{max}-l_{zero})}{(l_{zero})} \times \frac{1}{field}\left[\frac{nm}{V}\right] \times 1000[\frac{pm}{nm}] \tag{2.1}$$

Note that while this formula suggests a linear response of the piezoelectric response to the applied electric field, there is no guarantee that all molecules will exhibit linear electromechanical response. Depending on the molecule that is being examined, steric crowding or other large energetic barriers may exist, limiting the range of motion and distorting the linear piezoelectric nature.

2.2   SELF-ASSEMBLED MONOLAYERS

2.2.1   Sample preparation.

Gold-thiol monolayers are prepared using 1.0 mM solutions of dodecanethiol in ethanol or peptide in distilled water. These solvents are chosen due to solubility and have no impact on

the production of the monolayers. The substrates are gold metal on glass and cleaned by washing with ethanol and water followed by sonication for 10 minutes in ethanol or water for the alkanethiol or peptides, respectively. After cleaning, the substrates are dried with compressed air or N_2 and placed into the solution to sit for 24 hours to form an ordered monolayer. The substrates are then taken out of the solution and rinsed three times with the respective solvent, blown dry, covered, and placed in a desiccator until ready for analysis.

2.2.2   (AFM) / (PFM) analysis.

AFM and PFM measurements are performed using an Asylum Research MFP-3D SPM. Semi-quantitative piezoelectric results can be obtained by using the dual-AC resonance tracing (DART-PFM) mode. Gold-coated tips (TR400PB, Olympus) are used for the DART-PFM characterization. These tips have a free-air resonance frequency of 10 kHz, but a contact resonance of 35 kHz. The low spring constant of 0.02 N/m is significant due to the soft nature of the organic and biomaterials. A tip-sample bias of 1.5 - 4 V is applied for each sample to increase the quantitative nature of the technique. Topography, piezoresponse amplitude, and phase images are all recorded. The recorded amplitude is q-corrected to take the tip-sample resonance amplification DART-PFM utilizes into account. This q-correction is performed using the default analyzing software. Each sample is measured at least three times for consistency. For an increased quantification of the piezoelectric coefficient, each sample is examined over a range of voltages from $1.5 - 4.0$ V nm^{-1}.

3.0   SINGLE-MOLECULE PIEZOELECTRIC CALCULATIONS

The author performed the calculations for the phenanthrenes, Hammett-Taft correlations, and completed the functional group calculations for the [6]helicene backbone.

3.1   INTRODUCTION:

Piezoelectrics are polar materials that produce electrical charge in response to a mechanical distortion (the direct effect) or change shape in response to an applied electric field (i.e., the converse effect). Piezoelectrics differ from other shape-changing materials in that they exhibit a continuous, reversible linear shape change in response to an applied field, not a binary switching behavior like redox transitions[48,49] or reports of conformational changes in proteins based on STM.[50] As such, piezoelectrics have achieved use as combined sensors and actuators for applications as wide-ranging as sensors,[51,52], field effect transistors,[53] nanogenerators,[54,55] ultrasonic motors,[56] and scanning-probe microscopy manipulation.[57,58] A variety of conventional piezoelectric bulk materials are known, including perovskite materials such as lead zirconium titanate ($Pb[Zr_{1-x}Ti_x]O_3$ or PZT),[51,52,59] polyvinylidene difluoride (PVDF) and other

semicrystalline polymers,[51,60,61] quartz, and some liquid crystals.[51] Recent investigation into ZnO piezoelectric nanowires has demonstrated the ability to generate electrical power (up to 0.78 W/cm^3 when integrated into textiles) through energy harvesting.[62-64]

The piezoelectric property of PZT and ZnO single crystals stems from the accumulative dipole of each asymmetric unit cell,[65] and piezoelectric PVDF is achieved via a poling process in which polymer microcrystals are oriented to a uniform direction.[66] In this contribution, we first report an initial computational exploration of single molecules to serve as piezoelectrics/piezoelectric units. Regioisomer effects and the development of structure/property relationships for improved molecular piezoelectric materials are included. In particular, we focus on asymmetrically substituted donor-acceptor [6]helicenes and tetrahydrophenanthrenes, Figure 3.1.
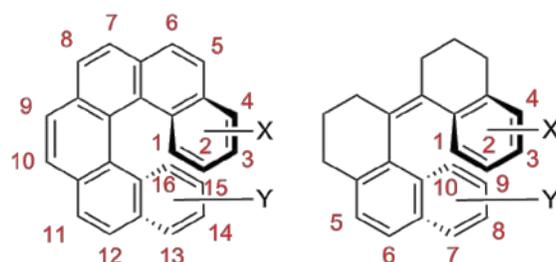
Figure 3.1. (left) [6]helicene backbone. (right) phenanthrene backbone.

These molecules and their derivatives are considered potentially useful in the field of asymmetric catalysis,[20,24] nonlinear optics,[67] molecular switches and rotors,[68,69] and thin film transistors.[70] With a spring-like and highly polarizable shape, as we will show, asymmetrically-substituted [6]helicenes and tetrahydrophenanthrenes respond to an applied electric field with a conformational deformation along the long axis (i.e., a converse piezoelectric effect) and change

polarization in response to a geometric distortion (i.e., a direct piezoelectric effect). Results and Discussion.

3.2   HELICENES.

In this paper, we will first discuss the substituted fully conjugated [6]helicenes and build a set of structure/property correlations. We will describe different regiochemical isomers using amino and nitro substituents, functional group substitutions in the 4- and 15- position, along with dipole moment and polarizability contributions to potential energy. The electric field was applied along the direction of C2 to C15, Figure 3.1, and is defined as the z-axis of the system. The field was varied between ±1.29 V/nm, large on macroscopic terms, but small on an atomistic scale, corresponding to the field due to an extra positive or negative charge at 1.06 nm from the molecule. Over the field range, the distance between the two nitrogen atoms was predicted to vary from 4.869 Å to 5.480 Å (corresponding to -1.29 V/nm and +1.29 V/nm applied field, respectively) as illustrated in Figure 3.2. This deformation of 0.61Å corresponds to ~12.5% length change and a computed piezoelectric constant d_{33} of 45.8 pm/V, comparable to 9.9~26.7 pm/V for ZnO piezoelectric materials.[71,72] Such a large d_{33} implies that much smaller fields, comparable to conventional piezoelectrics, can be used in experiments or practical applications. Between atoms C2 and C15, a deformation of 0.22Å also occurs, as illustrated in Figure 3.3, indicating that the molecule performs a complete structural change beyond a simple bending of the C-N amine and nitro groups. Molecules will be referenced so that position and functional group is clear, such as 4-amino-15-nitro[6]helicene is **4a15n**.

19
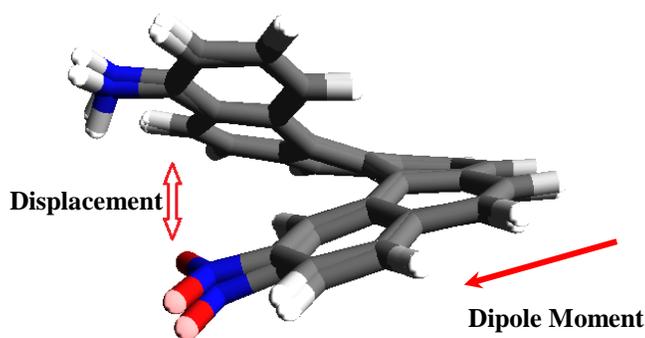
Figure 3.2. Superposition of [6]helicene 4a15n under two levels of applied field strength (±1.29 V/nm).
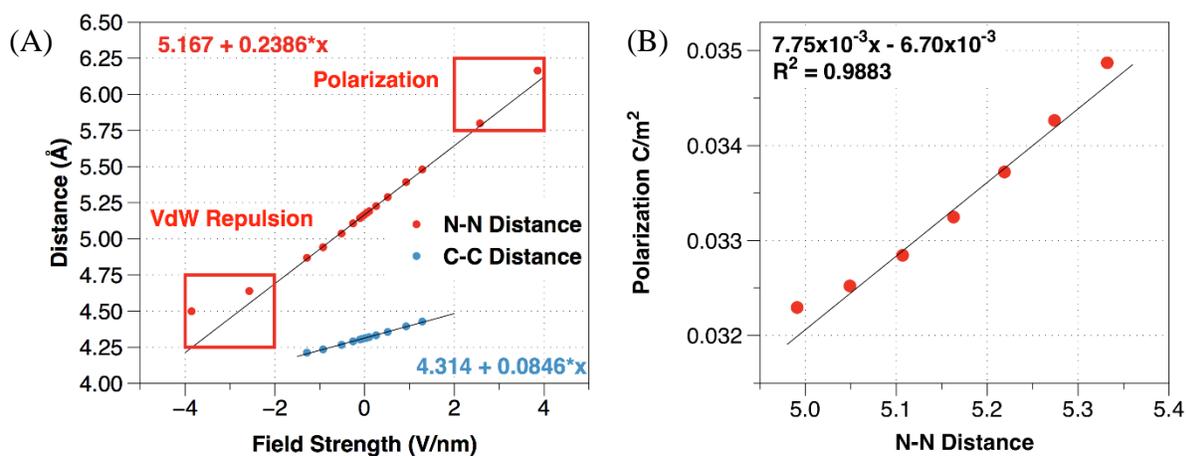
Figure 3.3. (A) Calculated N to N and C2 to C15 distances in 4a15n under different applied external electric fields demonstrating the converse piezoelectric effect. Note that while the deformations are largely linear across the field strengths studied, some curvature does occur at high positive and negative applied fields. (B) Calculated polarization (dipole moment per volume) in 4a15n at different constrained geometries, demonstrating the direct piezoelectric effect. Similar nonlinearities are found at large deformations.

As observed in Figure 3.3(A), molecules exhibit a converse piezoelectric effect, and while the variation in displacement is largely linear with applied external field, at large positive and negative fields some nonlinearity is found. During contraction with a negative field, the

20

molecular length begins to saturate beyond ~1.29 V/nm because of Van der Waals repulsion between atoms in the helicene. As the molecule extends with a large positive field, the π-electron polarization increases and slightly increases the deformation above linear response for fields beyond +1.29 V/nm.

Similarly, Figure 3.3(B) demonstrates a direct piezoelectric effect, found by calculating both the molecular dipole moment and van der Waals volume to give a polarization, at specific geometric distortions. For each N-N (or C2-C15) distance, the carbon atoms were set to a specific displacement and "frozen" for a constrained geometry optimization while all other atoms relaxed. While the dipole moment derives from separated charges, clearly partial charges redistribute as the conformation changes, yielding some nonlinearity, particularly at large geometric distortions. Thus, single molecules clearly exhibit both direct and converse piezoelectric effects. The remainder of the paper will discuss the converse effect, since its calculation does not require arbitrary geometric constraints.

The piezoelectric response of the molecule is due to coupling between the molecular dipole moment and the applied field, which changes the potential energy surface of the molecule and creates a new global minimum energy geometry. Equation 3.1 describes the energy change upon interaction with an external electric field of these systems: μ is the dipole moment, (C m^{-1}); $\vec{F}$ is the applied electric field, (V nm^{-1}); α is the polarizability of the molecule (C^2 m^2 J^{-1}); and β is the hyperpolarizability, (C^3 m^3 J^{-2}):

$$E(F_z) - E(F_z = 0) = \mu_z F_z + \alpha_{zz} F_z^{\,2} + \beta_{zzz} F_z^{\,3} \tag{3.1}$$

For the 4-amino-15-nitro[6]helicene (**4a15n**), the calculated energy change is 4.6 kJ/mol with 59% and 41% contributed from the dipole moment and polarizability, respectively and only 0.07% from the hyperpolarizability.
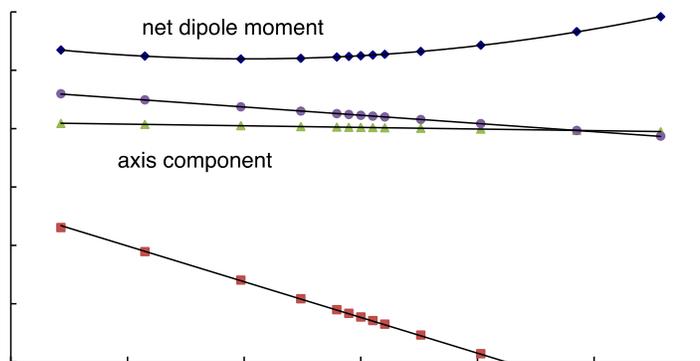
Figure 3.4. Computed net dipole moment along with the x-, y-, and z-axis components.

If we assume this energy excites only the lowest-energy breathing mode of the helicene (computed frequency of 31.4 cm^{-1} and computed force constant of 0.0045 mdyne $Å^{-1}$), the overall harmonic deformation would be over 1.84 Å! Clearly, multiple vibrations are excited, and immense electromechanical response is possible even with a relatively small potential energy change (4.6 kJ/mol). Figure 3.4 illustrates the non-monotonic change of the overall molecular dipole moment. At about -0.5 V/nm, the dipole moment reaches a minimum and increases as electric field increases or decreases. This effect derives from the near-orthogonality of the applied electric field and the dipole moment, illustrated in Figure 3.2. If each component of the dipole moment is considered (as in Figure 3.4), the z-axis component is affected most by the applied field, and at large field strength, dominates the overall dipole moment.

3.2.1   Regiochemical Isomers.

Beyond **4a15n,** all 16 amino-/nitro- regioisomers of [6]helicene, reflecting substitution at each of the 4 free positions of both the "top" and "bottom" rings in Figure 3.1, have been studied

22

for their predicted piezoelectric response. For each isomer, the geometry was optimized under a varying applied external electric field as described above. The length changes described are defined as the average change in length between the substituents from the molecule at 0 V/nm applied field to the lengths at ±1.29 V/nm. In all cases, a length deformation was found proportional to the magnitude of the field and the predicted piezoelectric coefficients are compiled in Table 3.3.1.

Table 3.3.1. Computed piezoresponse (d_{33}) of 16 isomers of amino- and nitro- substituted [6]helicenes.

Isomer	1a13n	1a14n	1a15n	1a16n	2a13n	2a14n	2a15n	2a16n
d_{33} (pm/V)	12.7	10.5	7.4	1.8	39.9	37.0	23.1	6.7
Isomer	3a13n	3a14n	3a15n	3a16n	4a13n	4a14n	4a15n	4a16n
d_{33} (pm/V)	23.5	44.7	36.7	6.1	13.5	23.7	48.8	8.3

The molecular geometry plays a large role in determining the overall deformation potentials. For example, in isomer **1a16n**, substituents on C1 and C16 are extremely close and likely form an intramolecular hydrogen bond between the $-NH_2$ and $-NO_2$ groups, restraining the molecule from significant contraction (due to steric repulsion) or extension, giving the smallest response in the series, 1.8 pm/V. Retaining only one substituent on C1 or C16, as in the isomers **1a15n**, **1a14n**, **1a13n**, **2a16n**, **3a16n** and **4a16n**, allows larger space for the molecule to extend and contract, so larger deformation is observed. The five isomers that exhibit a maximum deformation above 30 pm/V are **2a14n** (37.0 pm/V), **3a15n** (36.7 pm/V), **2a13n** (39.9 pm/V), **3a14n** (44.7 pm/V) and **4a15n** (48.8 pm/V). In these molecules, the two substituents are along

the lowest energy breathing mode, yielding a large z- component of the dipole moment and little steric repulsion.

For anisotropic properties such as piezoelectric response, the deformation of a material depends not only on the strength of the applied field, but also on the direction. We considered applied fields along multiple directions, since each molecule is inherently asymmetric, using field strengths between ±1.29 V/nm. Larger deformations take place when field is applied along or close to the z-axis, along the molecular breathing mode, see Figure 3.4 and Figure 3.5. For most of the 16 isomers, the largest deformation occurs when the field is applied along the C2 to C15 axis.
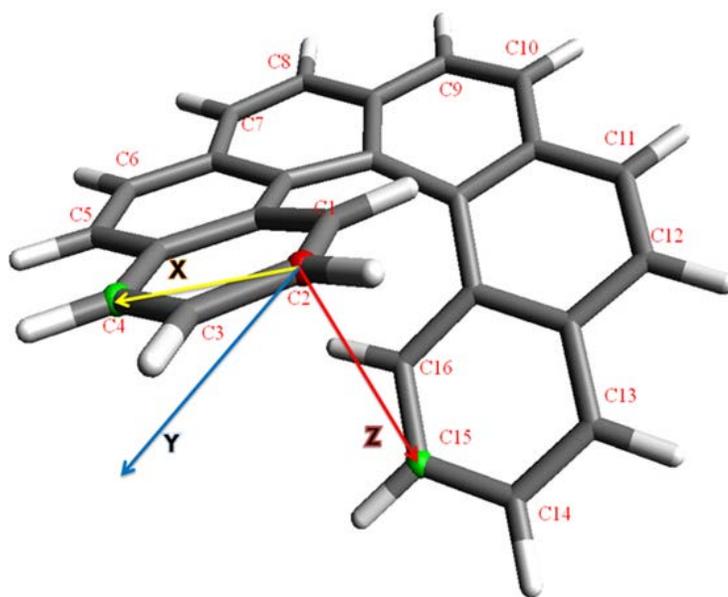
Figure 3.5. Internal coordinate of a helicene structure with numbering of atoms.

3.2.2 Dipole moment.

To optimize single-molecule piezoelectric response, one might imagine a larger dipole moment would give a larger geometric distortion. As discussed above, only the z-component of the dipole moment is directly coupled to the applied field, and in the 16 regiochemical isomers considered here, it is only a small component of the overall dipole moment. Consequently, there is little correlation between the molecular dipole moment and the deformation, or even in the magnitude of the z-component. As illustrated in Figure 3.6, there is some small correlation between the *fraction* of the overall dipole moment in the z-direction at zero applied field and the piezoelectric deformation.
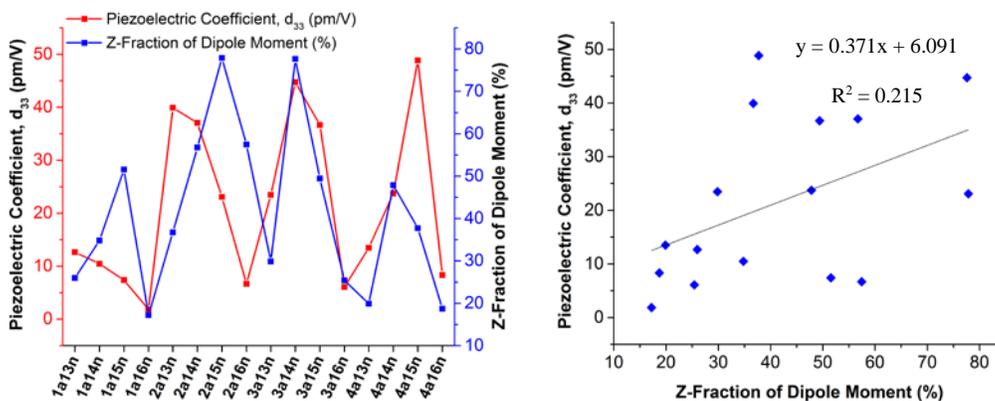
Figure 3.6. (left) Calculated z-fraction dipole moment and d_{33} of regiochemical isomers. (right) Piezoelectric response correlation with z-fraction of dipole moment.

3.2.3 Functional groups.
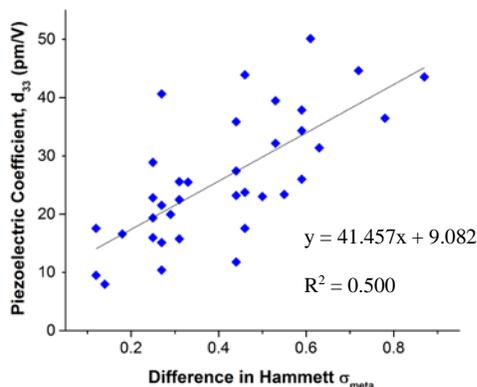
Figure 3.7. Correlation between d_{33} and the difference between the functional groups' Hammett σ_{meta} for [6]helicene.

Several activating and deactivating functional groups with varying strength were studied, resulting in 36 different 4- and 15- substituted [6]helicenes using a combination of 6 electron withdrawing and 6 electron donating groups, with computed piezoresponse compiled in Figure 3.8. Although IUPAC numbering would change depending on what functional group is attached to the helicene, the numbering will be kept consistent with Figure 3.1 to limit possible confusion. Hammett-Taft parameters were used for the σ_{meta} constants to determine the difference in electronic directing character.[73,74] In Figure 3.7, a strong correlation between the calculated piezoelectric response and the difference in Hammett-Taft constants ($\Delta\sigma_{meta}$) is observed. However, a combination of a strong electron withdrawing group and a strong electron donating group doesn't insure a large z-fraction of dipole moment. The relationship of deformation and z-fraction dipole moment is vague in these isomers, but with a stronger electron withdrawing group and stronger electron donating group, the z-fraction of dipole moment changes less, which

26

means those molecules favor a shape deformation rather than charge redistribution under the applied field.
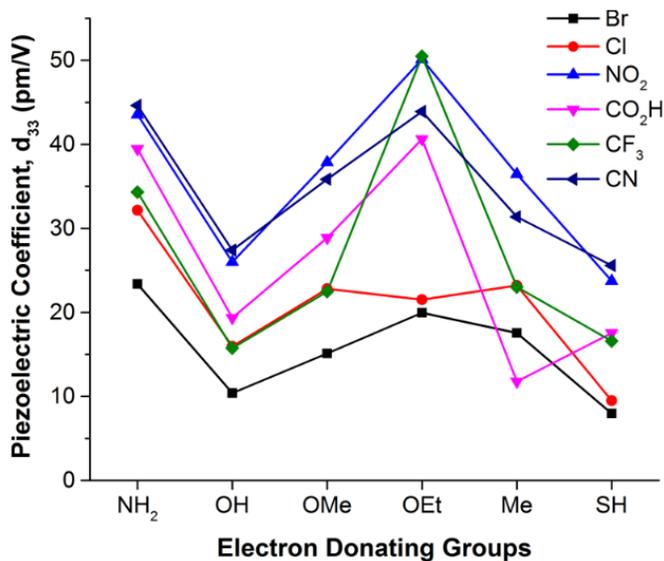
Figure 3.8. [6]Helicene piezoelectric response, d_{33}, with respect to varied electron donating and withdrawing functional groups.

3.2.4 Polarizability.

The regiochemistry clearly complicates the correlation of molecular dipole moment and computed piezoresponse. The high degree of correlation, however, between the difference in Hammett parameters and predicted piezo coefficient suggests that higher dipole moments generally yield greater geometric deformation. Figure 3.9 shows the relationship between computed polarizability and deformation of the 16 amino- and nitro- substituted helicenes. While the correlation is slightly higher than with the dipole moment, the regiochemistry also

complicates the response. Instead, one can consider a series of elongated helicenes, adding more fused benzene rings to linearly (i.e., rather than helically) extend the helicene. Such "clamphenes" show dramatically increased geometric deformation (Figure 3.10), deriving largely from their increased polarizability.
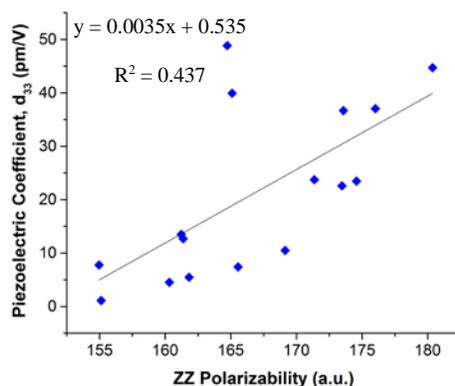
Figure 3.9. Correlation between d_{33} and ZZ polarizability for 16 regiochemical isomers of amino- and nitro-[6]helicene.

As an example, a hypothetical helicene derivative is proposed for single molecule piezoelectrics with high response, illustrated in Figure 3.10. This molecule could be considered as adding a naphthalene group to both ends of a [6]helicene, increasing the "arm length" and thus the linear distortion along the z-axis. For the clamp-like shape of the molecule, we name it 5-amino-20-nitro "clamphene" (**CP10-5a20n**), shown in Figure 3.10. As with the [6]helicenes, under an applied electric field range of ±1.29 V/nm, the computed distance between the two nitrogen atoms extends from 8.29 Å to 10.94 Å, yielding a 32% length deformation, and a computed d_{33} piezoelectric constant of 110 pm/V, comparable to many inorganic piezoelectric

materials.[51,52] As the arm length is further extended, the calculated d_{33} increases even further as seen in Figure 3.11.
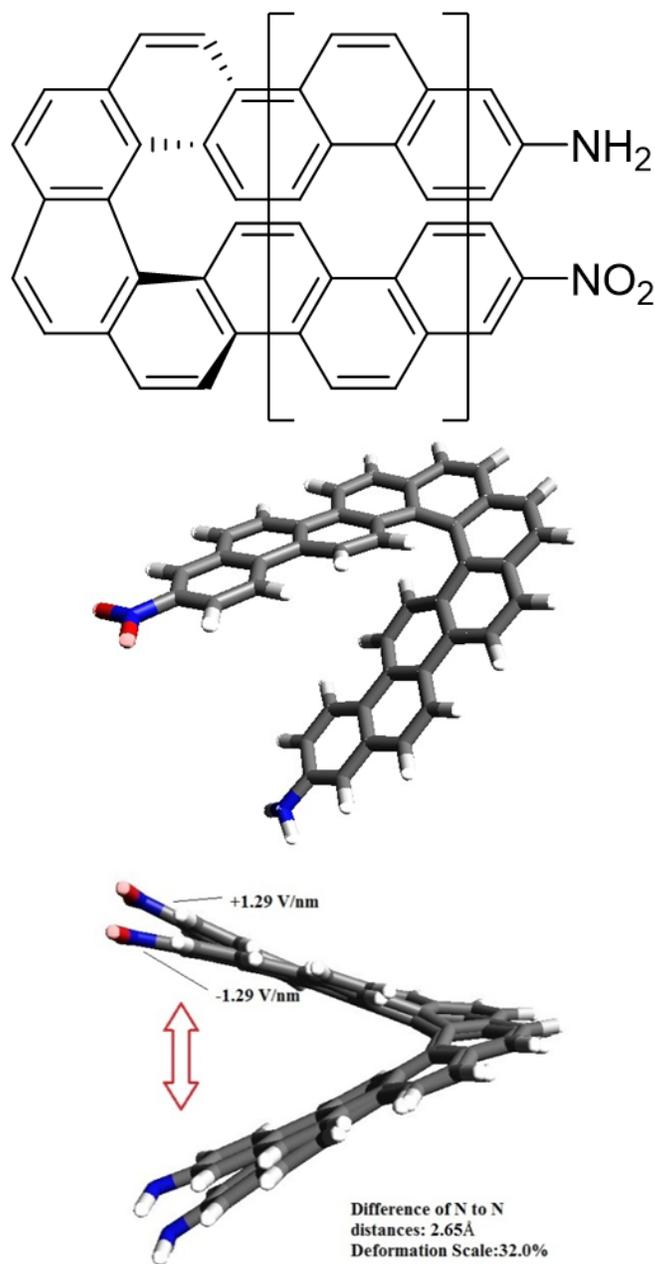
Figure 3.10. (top) Extended –arene used for polarizability and upper-limit calculations. (middle) Example "clamphene" 5-amino-20-nitro-"clamphene" (**CP10-5a20n**). (bottom) Computed deformation of **CP-10-5a20n**.
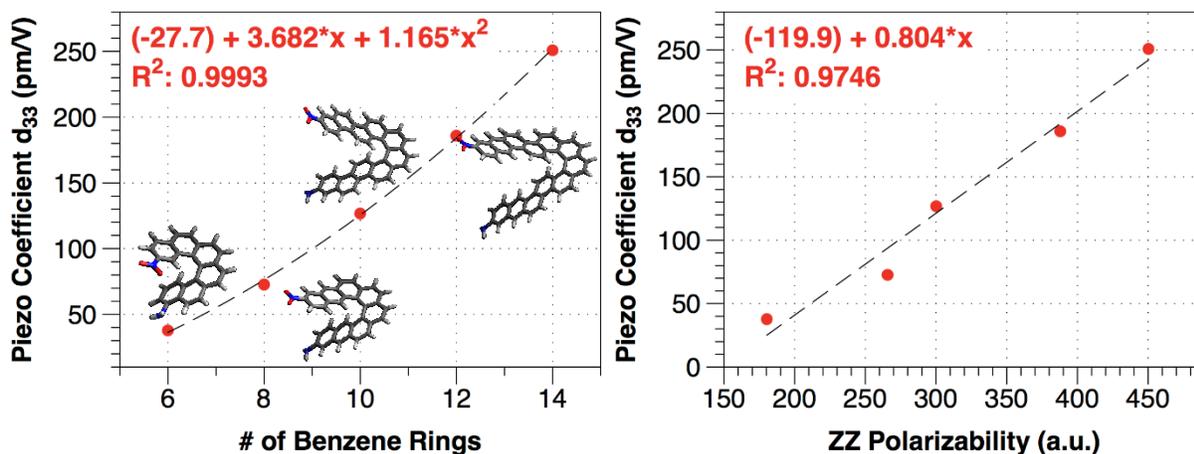
Figure 3.11. Increased computed geometric deformation (left) as a function of the number of benzene rings in the clamphenes and (right) as a function of the computed zz-component of the polarizability.

3.3   PHENANTHRENES.

The tetrahydrophenanthrene system is obviously a more flexible hinge due to the lack of conjugation in part of the system and the incomplete ring system allowing for larger piezoelectric deformations through a rotation around the double bond, but with the downside of potential *cis/trans* isomerization. For the phenanthrenes, a field is applied along C2 to C9 on which lies the breathing mode of the molecules. The same field range as [6]helicene, ±1.29 V/nm, is applied for all molecules studied. The distance between the first atoms on each functional group is used in the determination of the piezoelectric response. In terms of regiochemistry, polarizability, dipole moment, and functional group, the behavior of the substituted phenanthrenes under applied electric field is similar to that of substituted helicenes.

Similar to the [6]helicene above, the piezoelectric response of this phenanthrenes molecule is due to the coupling of the molecular dipole moment to the applied electrical field,

which modifies the potential energy surface of the molecule and creates a new global potential energy minimum. Using equation 3.1 above, the potential energy of the 3-amino-8-nitro-phenanthrene, **3a8n,** is 4.4 kJ/mol, with a contribution of 55% from the dipole moment and 45% from the polarizability, slightly higher than the calculated contributions for [6]helicene.

As with the [6]helicene above, if we take into account only the lowest energy breathing mode (computed frequency of 27.7 cm^{-1}, and computed force constant of 0.0030 mdyne $Å^{-1}$), the overall harmonic deformation would be over 2.21 Å. Even though the potential energy change is relatively small (4.4 kJ/mol), a large electromechanical change is possible, but again, multiple vibrational modes are excited at once.

3.3.1 Regiochemical isomers.

All 16 possible combinations of regiochemical isomers comparable to [6]helicene were tested for the phenanthrene. The geometry was optimized as described for the [6]helicene above. A larger piezoelectric response is noted for regiochemical isomers where the functional groups are along the breathing mode of the molecule and smaller responses are noted for molecules with the functional groups close to the center of the system as shown in Table 3.3.2**.**

Table 3.3.2. Computed piezoresponse (d_{33}) of 16 isomers of amino- and nitro- substituted phenanthrenes using an applied field of ± 1.29 V/nm along C1 to C10.

Isomer	1a7n	1a8n	1a9n	1a10n	2a7n	2a8n	2a9n	2a10n
d_{33} (pm/V)	17.9	14.5	8.6	1.1	40.9	34.2	21.9	2.7
Isomer	3a7n	3a8n	3a9n	3a10n	4a7n	4a8n	4a9n	4a10n
d_{33} (pm/V)	32.7	47.4	42.4	8.2	18.2	32.1	59.7	10.2

The molecular geometry plays a similar role in the phenanthrene system as it does in [6]helicene. A response greater than 40 pm/V is predicted for four of the isomers: **2a7n** (40.9 pm/V), **3a9n** (42.4 pm/V), **3a8n** (47.4 pm/V), and **4a9n** (59.7 pm/V). The substituents for these high deformation isomers are aligned mostly parallel with the applied field likely leading to a large affect from the field. The small responses, less than 10 pm/V, seem to be due to the increased distance between the substituents and the misalignment between the field and the functional groups.

3.3.2 Dipole moment.
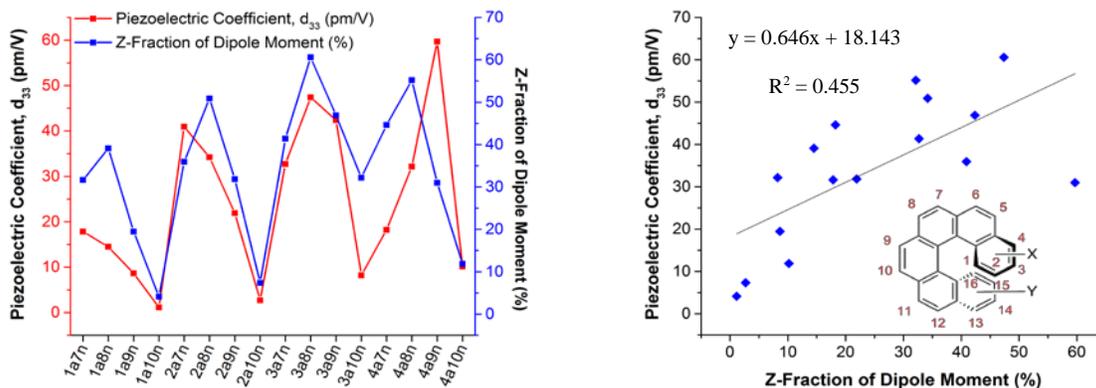
Figure 3.12. (left) Calculated piezoresponse (d_{33}) for 16 regiochemical isomers for amino- and nitro- substituted phenanthrene and z-fraction of the dipole moment of the 16 regiochemical isomers under an applied field of ±1.285 V/nm. (right) Correlation between d_{33} and the z-fraction of the dipole moment (%).

Just as [6]helicene, the z-component of the phenanthrene is directly coupled to the applied field. As seen in Figure 3.12 there is a much larger correlation between the z-fraction of the dipole moment for the phenanthrene and its piezoelectric response than [6]helicene. Of the 16 regiochemical isomers studied here, 13 have a contribution of over 50% from the z-component of the dipole moment.

33

3.3.3 Functional groups.

A variety of 3- and 8- substituted phenanthrenes were tested for their calculated piezoelectric coefficient, and although this regiochemical isomer does not show the highest calculated response above, the response of **4a9n** had a large variation over the ±1.285 V/nm range that it was tested, so for consistency purposes we decided 3- and 8- substituted phenanthrenes would be better experiments. Just as the [6]helicene above, in order to reduce confusion, the numbering will not match the IUPAC system, but instead will use the numbering in Figure 3.1. Longer alkyl and alkoxy groups exhibit a larger percent deformation that we suspect is due to the free rotation capabilities of these chains. Figure 3.13 shows the piezoelectric deformation of 42 combinations of functional groups tested. Figure 3.14 shows that generally stronger electron withdrawing groups (e.g., -NO_2 and -CN) and stronger electron donating groups (-NH_2 and -OR) will have larger deformation.
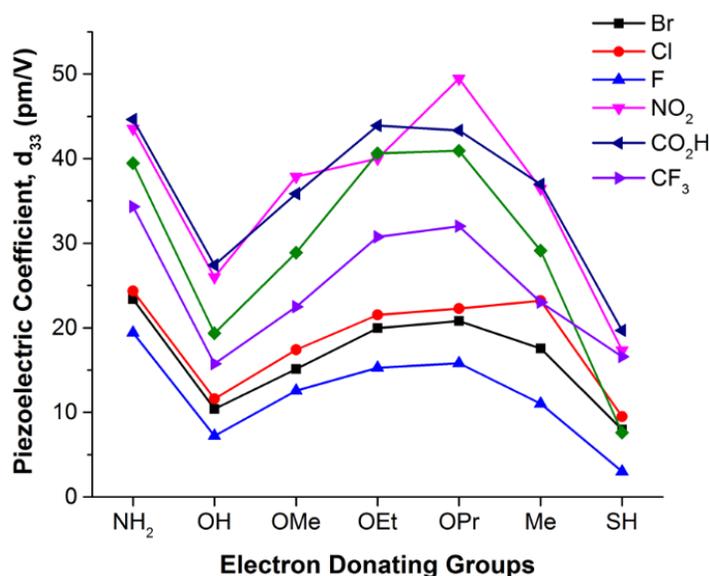
**Figure 3.13.** Phenanthrene piezoelectric response, d_{33}, with respect to varied electron donating and withdrawing functional groups.
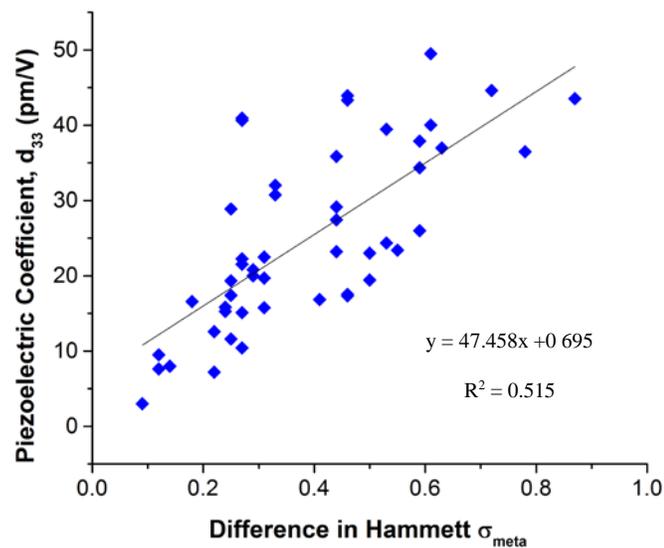
Figure 3.14. Correlation between d_{33} and the difference between the functional groups' Hammett σ_{meta} for phenanthrene.

3.3.4 Polarizability.
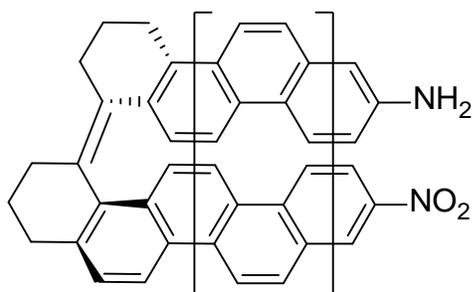
Figure 3.15. Extended –arene with phenanthrene skeleton used to show effect of polarizability on piezo-response.

Since the polarizability of these molecules contributes a large percentage to the potential energy of the "spring-like" system, then by increasing the polarizability a larger piezoelectric

response should be predicted. Extending the conjugated system of the phenanthrenes by increasing the number of fused aromatic rings, as seen in Figure 3.15, increases the polarizability of the molecule and in turn, the piezoelectric response. There is a very high correlation between the polarizability and the calculated piezoelectric coefficient, d_{33}, for the extended –arenes. With this relationship, we find that molecules that are highly polarizable are better targets than molecules with just a large z-component of the dipole moment based on the low correlation between z-component and the piezoelectric response as seen in Figure 3.16. There is a large correlation between both the extension of the system by increasing the number of fused aromatic rings and the ZZ polarizability with the piezo coefficient, d_{33}.

The reported responses might not be the highest for the systems of this size due to the regiochemistry of the functional groups. The position was chosen so the results were comparable between the extended –arenes.
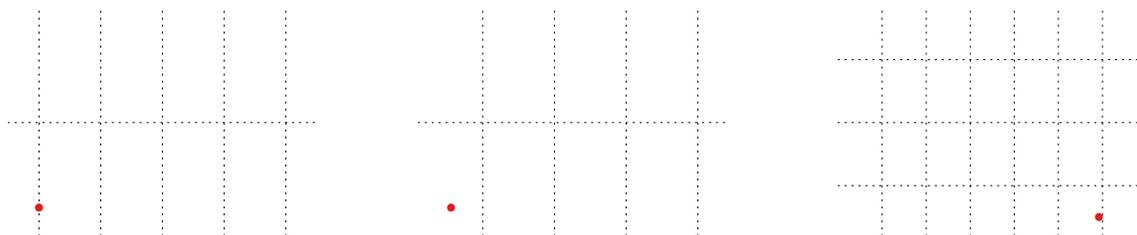
Figure 3.16. (left) The computed piezo coefficient of the molecule increases as the number of additional fused aromatic rings increases. This increase is correlated (center) to the increased polarizability (and thus induced dipole moment) and not the z-component of the permanent dipole moment (right).

3.4   CONCLUSIONS

We have demonstrated that single molecules can respond via piezoelectric distortion to an applied electric field. Such changes are conformational in nature, as the coupling between the applied field and the molecular dipole moment drive an expansion or contraction of the molecular helix, along the breathing modes. The applied field changes the global minimum geometry, on top of any vibrational displacements about the equilibrium.

Regioisomeric effects are found to be important, based on our study of 16 regioisomers of amino-nitro[6]helicene and phenanthrene. The regiochemical effect on the piezoelectric response is complicated, although we find a large predicted piezoelectric coefficient, $d_{33,}$ for several regiochemical isomers and a variety of substituted [6]helicenes and phenanthrenes, most notably 4-amino-15-nitro[6]helicene with a piezoelectric coefficient of 45.8 pm/V and 49.5 pm/V for 3-nitro-8-propoxy phenanthrene, both comparable with inorganic materials, and far above piezoelectric response in other organics, such as PVDF. Piezoelectric responses, upwards of 100-200 pm/V, have been predicted for the extended helicenes and phenanthrenes, or "clamphenes." It should be mentioned that these responses are measured on single molecules and not crystals nor multi-layers like conventional piezoelectric materials. We suspect that due to enhancement of the local electric field, deriving from aligned molecular dipole moments, multi-layer polar films may yield even greater response.[25]

Correlating dipole moment, polarizability, and steric interactions with the piezoelectric response will provide future design direction. Modification of the piezoelectric response is possible by changing the regiochemistry of these skeletons. In our study of substituted [6]helicene, a range of 47 pm/V (1.8 to 48.8 pm/V) is shown solely by modifying the positions of the substituents. The regiochemical effects are not completely clear but some initial reasoning

behind the noticeable differences includes steric inhibitions, intramolecular hydrogen bonding for certain substituents, and alignment with the applied electrical field. Preliminary studies have shown that as the difference in Hammett-Taft constants increases, the piezoelectric response also increases. Other design rules for good targets that have shown promise include high polarizability, since the polarizability contributes ~41% of the potential energy, and a low force constant to allow for larger deformations for lower input force.

From what we have shown, it is possible that there is little "upper limit" to the piezoelectric response of molecules designed for conformational response. For example, in order to generate a piezoelectric response of 500 pm/V, on par with lead zirconium titanate (PZT), a molecule would need only a 50% change in length upon an applied electric field of 1 V/nm (e.g. 4 Å to 6 Å). While such a target molecule has not yet been discovered, it is easy to imagine that such molecules can exist based on our computations of the extended systems, "clamphenes" and well-known redox-mediated conformational changes such as biological ion channels.

4.0   HETEROHELICENE SINGLE-MOLECULE PIEZOELECTRICS

This work was written in collaboration with Cameron Selby, Anjali Premkumar, and Geoffrey Hutchison*.

The author performed calculations and the complete analysis of the data.

4.1   INTRODUCTION

Building upon the results from the [6]helicene and phenanthrene computational study, it was noted that the polarizability of this class of materials has a large influence on the overall piezoelectric response. To further explore the effects of polarizability and electron density on the response of these systems, electron rich and electron poor heterocycles such as thiophene, furan, pyrole, and azacycles substitutions were placed along the backbone. These substitutions are common, organic heterocycles, making these computational targets no less synthetically accessible than the previous molecules.

Piezoelectrics are a class of materials that interconvert between electrical and mechanical energy. This conversion can be defined two ways: the direct effect, where the mechanical force is converted to electrical charge; and the converse effect, where an applied voltage bias causes a change of shape. These materials are unique in that the effect is continuous, linear, and reversible in response to an applied field or deformation. Consequently, there are a wide variety of uses for

piezoelectrics such as sensors,[75] field effect transistors (FETs),[53] actuators,[76] and nanogenerators.[77]

Some of the more common materials used for piezoelectric devices are the perovskite, lead zirconium titanate ($Pb[Zr_{1-x}Ti_x]O_3$ or PZT),[78] zinc oxide (ZnO),[64] and polyvinylidene difluoride (PVDF).[79] One of the inherent flaws of many piezomaterials, including PZT and PVDF, is a lack of an intrinsic piezoelectric capability, meaning the application of a high poling voltage (100 kV cm^{-1}) and temperature (120 ºC) is required in order to achieve an enhanced response.[78] Recently, a novel class of piezoelectric composite materials was developed which incorporates the flexibility of polyurethane foam with the tailorable properties of organic molecules.[80] These foam composites exhibit a piezoelectric response of up to 250 pC N^{-1} acquired through poling at significantly lower voltages (400 V mm^{-1}) than ceramics (10 kV mm^{-1}). The piezoelectric effect of PZT and ZnO arises from the aggregate dipole moments from the asymmetric unit cells after poling.[77] Taking these flaws into account, we proposed molecules for replacements for these conventional piezoelectrics because they are inherently polar and we discovered molecules that exhibit the piezoelectric property. Previous work found that the piezoelectric response of the functional and regiochemical derivatives of [6]-helicene (maximum 45.8 pm/V) and tetrahydrophenanthrene (maximum 54.3 pm/V) in which it was noted that the piezoelectric response can be maximized by changing the substituents and the regiochemistry.[81]

In this report, examination of the single molecule piezoelectrics is continued by thoroughly exploring the effect of substitution in the backbone with heteroatoms such as nitrogen, oxygen, and sulfur leading to a modification of steric properties of the end rings in [6]- and [7] helicene. We show an increase from 54.3 pm V^{-1} upwards to 108 pm V^{-1} for the heteroatom substitutions that were made, doubling the previously computed results. Unlike

conventional piezoelectric materials, the compounds discussed here achieve the piezoelectric property from having an asymmetric molecular shape instead of a non-centrosymmetric crystal structure. This difference allows for the compounds to exhibit the piezoelectric effect as a monolayer without the need for high-voltage to achieve the piezoelectric character.

4.2   RESULTS AND DISCUSSION

4.2.1   Heterocycle substitutions.

This chapter will first discuss the effect heteroatom substitutions have on the piezoelectric coefficient, d_{33}, when substituted along the backbone. This study was limited to nitrogen, oxygen, and sulfur, atoms that are commonly found in organic molecules. An external electric field was applied along the direction of C_1 to C_{16} which is defined as the z-axis for calculations. This field was varied along ± 1.285 V/nm to produce an accurate representation of the linear piezoelectric property.
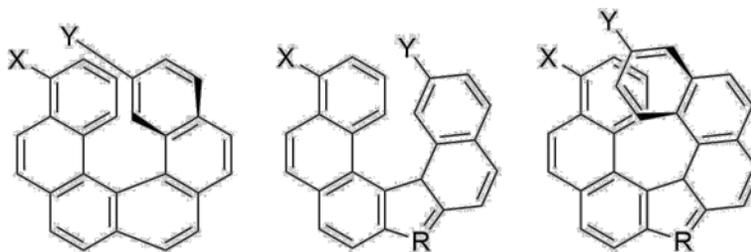
Figure 4.1. Structure showing the orientation of functional groups for (left) [6]helicene, (middle) [6]helicene with a heterocycle, and (right) diphenanthrenyl heterocycle.

Common organic heteroatoms were substituted in multiple positions using both [6]- and [7]-helicene backbones. The [6]-helicene backbone was used when only the end rings were modified in the case of pyridine and other aza-substituted ring systems. For the other modifications, a 5-membered heterocycle was added along the backbone to accommodate for the change in the structural relationships of the $-NH_2$ and $-NO_2$ functional groups to allow for the highest amount of alignment along the direction of the applied electric field as seen in Figure 4.1.

4.2.2 Single heteroatom substitution.
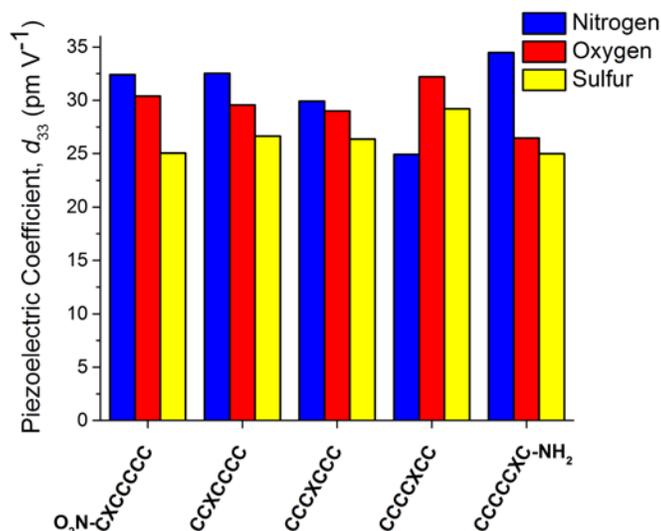
Figure 4.2. Comparison of the piezoelectric coefficient of pyrrole, furan, and thiophene [7]-helicene.

The heteroatom modifications made here affect the helicene by changing the overlap of the end-ring locations, so another ring is needed to align the functional groups. The angle between the functional groups R_1 and R_2 and the backbone differs by less than 10% with respect to both the [6]- and [7]-helicene motifs. That said, both the oxygen and nitrogen heterocycles had a larger piezoelectric response than the corresponding all-carbon helicene for each location as

seen in Figure 4.2. The average response for nitrogen, 30.9 pm V^{-1}, is 4.5% greater than the response of oxygen, 29.5 pm V^{-1}. Both nitrogen and oxygen consistently have larger piezoelectric responses than the sulfur analog, 14% and 10% respectively, and the larger responses for the non-sulfur heterocycles can be attributed to the larger size of the sulfur atom causing a greater misalignment of the functional groups. In the case of CCCCXCC, where nitrogen has a lower response than both oxygen and sulfur, the dihedral angle between the functional groups is ~90°, compared to 30-35° for every other case. This large dihedral angle shows a misalignment of the functional groups, thus lowering the overall piezoelectric response. All three of the heterocycles had responses between ~25 – 30 pm V^{-1}, which is within the same range as conventional polyvinylidene difluoride piezomaterials. The π-electron rich nature of these three heterocycles is likely the leading cause of the variation of the responses from the all-carbon [6]helicene. This increased electron density of the backbone allows for a larger movement of electrons and an increased piezoresponse.

4.2.3   Two-atom substitution.
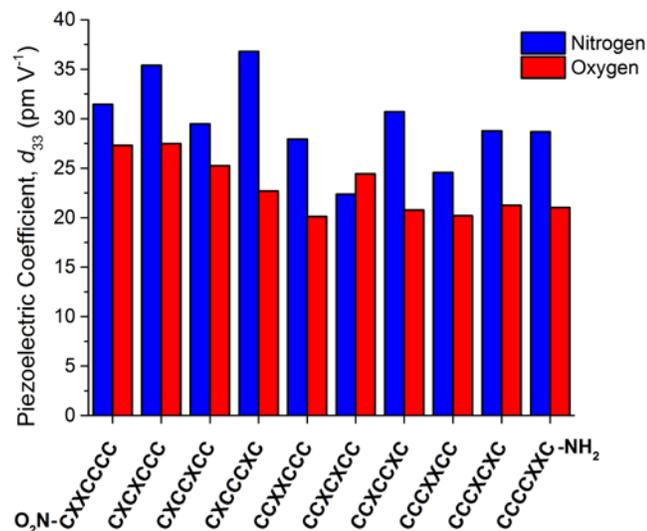
Figure 4.3. Two heterocycle substitutions implemented in the [6]helicene motif.

The oxygen and nitrogen heterocycles showed the greatest responses in the calculations above, so the inclusion of sulfur is deemed fruitless since a goal of this research is the optimization of the piezoelectric response. By adding in a second heterocycle into the [6]helicene motif, the nitrogen substitutions showed similar average responses, 23 pm V^{-1}, however, there were a few responses larger than the single substitutions, 36.8 and 35.4 pm V^{-1}. With nitrogen on the first end ring, the responses were greater than the single substituted helicenes, 33 versus 30.9 pm V^{-1}. The average response for the double nitrogen substitutions in comparable to the average for the single heteroatoms, 29.6 and 30.85 pm V^{-1}, a difference of 4.2%. However, for the case of oxygen, the overall responses were lower than the single-heterocycle molecules, 23.1 versus 29.5 pm V^{-1}, a difference of 28.1%. Analogous to the single substitutions, the addition of the second

44

furan ring causes a larger misalignment of the functional groups due to the increased size of the oxygen versus the nitrogen.

4.2.4   Azahelicenes.
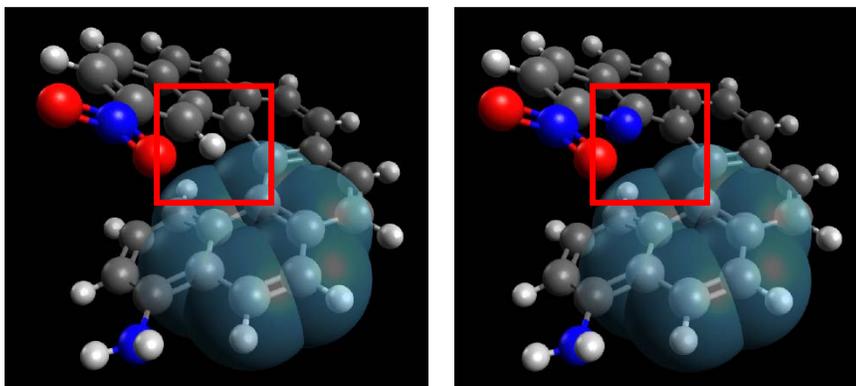
Figure 4.4. Left: 4-amino-15-nitro[6]helicene. Right: 4-amino-15-nitro[6]-azahelicene. Presence of H-atom which interacts with π-system of other half of the backbone.

Due to the largest responses being from when nitrogen atoms were the primary substituted heteroatoms, the next logical course of action was to increase the number of nitrogen substitutions made. We focused on the end groups of the helicene since substitutions in these locations appeared to have the largest impact on the overall piezoelectric response. Discussing only the top candidates, it appears that the steric hindrance that comes with having the hydrogens directly above or below the opposite end ring causes a decrease in the available range of motion. When one or both of these hydrogens are removed, Figure 4.4, the piezoelectric response is greatly improved. Modifying the end ring to incorporate nitrogens affects the dipole of the entire system as well, but it appears that the steric effect is the major cause of this large piezoelectric response.
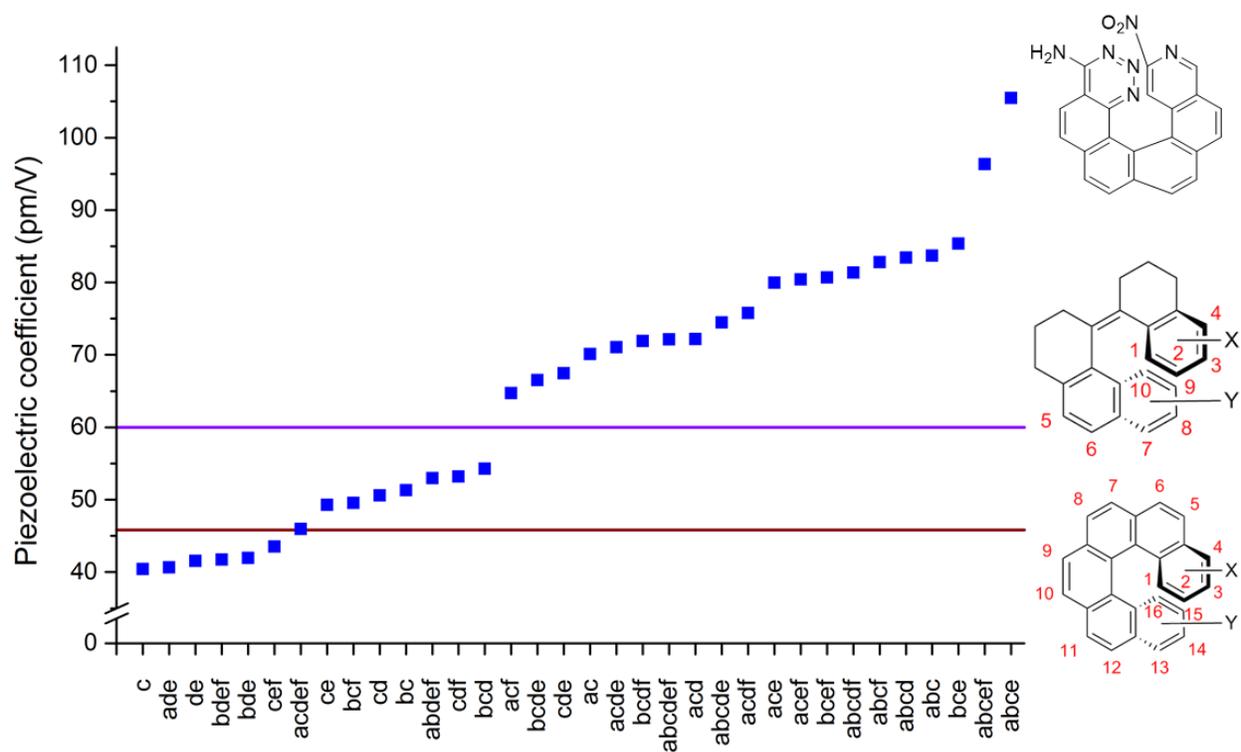
Figure 4.5. Piezoelectric coefficient, d$_{33}$, of azahelicene molecules with responses greater than 4-amino-15-nitro[6]helicene. Lines indicate largest responses for (red): [6]helicene and (purple): phenanthrene from previous study.

The lack of a proton in the highlighted region allows for a wider range of motion due to a lack of electrostatic interaction and an increased piezoelectric response, as shown in Figure 4.5 The largest response was seen in the azahelicene, 108 pm V^{-1} for abce, which removes two hydrogens that overlaps the π-system of the other half of the ring. This response sets the record for the largest computed molecular piezoelectric response and is also greater than the known responses of $BaTiO_3$, 75 pm V^{-1}, PVDF, -28 pm V^{-1}, ZnO, ~30 pm V^{-1}, and our computed 4-amino-15-nitro[6]helicene response of 45.8 pm V^{-1}.

4.2.5   Dipole moment and polarizability
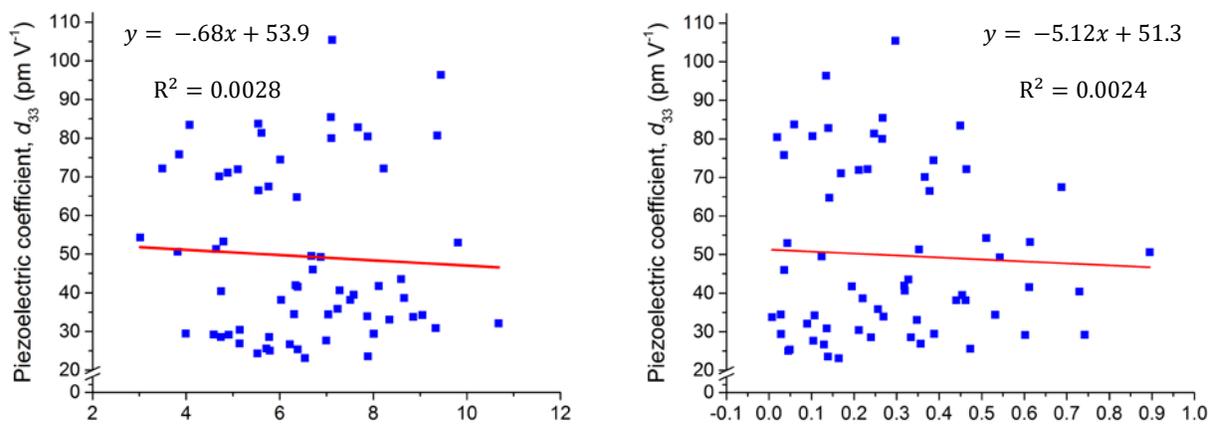
Figure 4.6. Correlation between piezoresponse and dipole moment (left) and z-fraction of dipole moment (right).

In the search for the cause for the increased piezoelectric response of the azahelicene derivatives, the influence of the dipole moment was examined. The correlations between the overall dipole moment, the z-fraction of the dipole moment, and just the z-component were all analyzed as shown in Figure 4.6. The low correlation between the overall dipole moment and the

piezoelectric response was no surprise because there needs to be a large alignment between the dipole moment and the lowest energy vibrational mode as shown Chapter 3. The low correlation of the z-fraction and the z-component of the dipole moment was unexpected since previous results suggested a significant correlation between these two factors. The z-component of dipole moment suggests a negligible influence on the piezoelectric response suggesting a much larger contributor must be present.
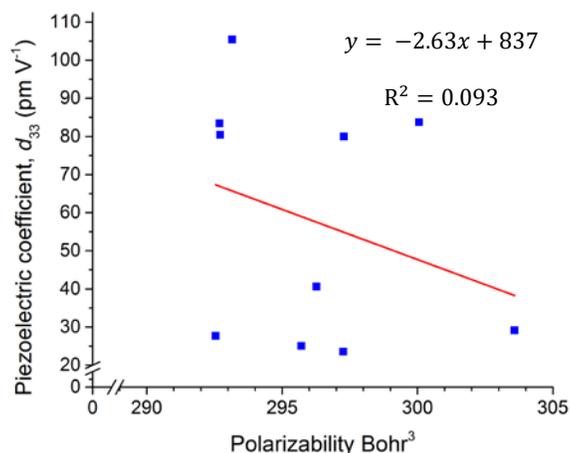
Figure 4.7. Correlation of polarizability with piezoelectric response of top 10 azahelicenes.

Progressing from the dipole moment, examination of how the polarizability influences the piezo response is next logical step. As seen in Figure 4.7, although the polarizability shows a larger correlation with the piezoresponse than the dipole moments do, the correlation is still lower than the pure carbon [6]helicenes previously studied. The low correlations between the piezoelectric coefficient and z-fraction of dipole moment and the polarizability, respectively, still alludes to a broader reasoning for their increased responses.

Through careful analysis of the locations of the nitrogen substitutions, a few key observations can be made: it is beneficial to substitute the carbon in the "c" location; substitution in the "e" position has almost no influence on the piezoelectric response, and substitutions in the "d" and "f" position decrease the piezoelectric response.

Table 4.1. Analysis of effect location of nitrogen substitutions have on piezoelectric response of azahelicenes.

Instance	Adding a substitution to position _	To a molecule with a substitution in position	Causes the response to _____.	Number of applicable molecules	Exceptions
1	A	c	Increase	14	cde, cdef
2	A	Not c	Decrease	15	None
3	B	cde, not a	Decrease	2	None
4	B	ad, not c	Decrease	4	None
5	B	Not **3** or **4**	Increase	24	ae
6	C	Anything	Increase	30	bdef
7	D	Not b, not both a and c	Increase	11	None
8	D	bf, not both a and c, not e	Increase	3	None
9	D	be, not a, not c	Increase	2	None
10	D	Not **7**, **8**, or **9**	Decrease	15	None
11	E	acd	Decrease	4	None
12	E	cdf, not a	Decrease	2	None
13	E	Not **11** or **12**	Increase	25	None
14	F	d, not e	Increase	7	abcd
15	F	bde, not c	Increase	2	None
16	F	Not **14** or **15**	Decrease	21	None

4.3   CONCLUSIONS

Expanding upon our previous work on the [6]helicene scaffold, backbone modifications have shown a considerable increase in the computed performance of the single-molecule piezoelectric compounds. Through the addition of heterocycles to [6]helicene, multiple characteristics of the molecular spring which impact the piezoelectric property are changed, such as the alignment of the polar functional groups and the overlap of hydrogens with the π-system, contributing to the largest computed response of 108 pm/V. These characteristics show that the piezoelectric response is affected just as much by the flexibility and alignment of the system as it is of the dipole moment and polarizability.

Of the systems tested, the largest piezoelectric response came from a conventional [6]helicene backbone with nitrogen substitutions in the end rings. The substitutions which removed a hydrogen that restricted the range of motion of the spring allowed for a larger computed response. The addition of heterocycles to the [6]helicene scaffold affected the piezoelectric response as well, however not in a favorable manner. Through these computations, we conclude that even though electron-rich heterocycles lead to an increased electron density of the conjugated system, the flexibility of the system impacts the response in a much larger manner.

5.0   QUANTITATIVE ASSESSMENT OF PIEZOELECTRIC PEPTIDES

This work was performed in collaboration with Haley Grimm, Nathaniel Miller, Seth Horne, and Geoffrey Hutchison*.

The author performed the PFM and DART-PFM measurements for this project.

5.1   INTRODUCTION

The previous computational experiments elucidated that increased dipole moment, polarizability, and reduced steric effects have the largest influence on the piezoelectric response of single-molecule piezoelectric materials. Since asymmetric [6]helicene is a difficult synthetic target to approach, different synthetically accessible targets were chosen: peptides. Having access to both natural and unnatural amino acids, the dipole moment and helicity of peptides can be tailored to fit most desired parameters. The tailorability and building-block approach to the synthesis of peptides also allows for the synthesis of a set of peptides to directly test the influence helicity or dipole moment have on the response by forming and characterizing self-assembled monolayers (SAMs) of these peptides.

This chapter discusses the quantitative determination and the origin of the piezoelectric property in a series of α-peptides utilizing circular dichroism (CD), Fourier-transform infrared (FTIR) spectroscopy, X-ray photoelectron spectroscopy (XPS), and piezoresponse force

microscopy (PFM). From our computational studies, we found that the spring-like structure of the helicenes allows for a large piezoelectric response. Peptides also exhibit the spring-like, helical structure through an α-helix secondary structure. Modified peptides are more synthetically accessible than comparable tailored helicene derivatives. Using the results from our computational studies, 2 sets of peptides were synthesized for the quantitative assessment of their piezoelectric property when formed into self-assembled monolayers (SAMs). These sets differ by whether they attach to the gold surface at the C- or the N-terminus, as seen in Figure 5.1. The hypothesis for this work is that by modifying α-peptides to have varying degrees of helicity, a correlation can be found between the helicity of the peptide and its piezoelectric response.
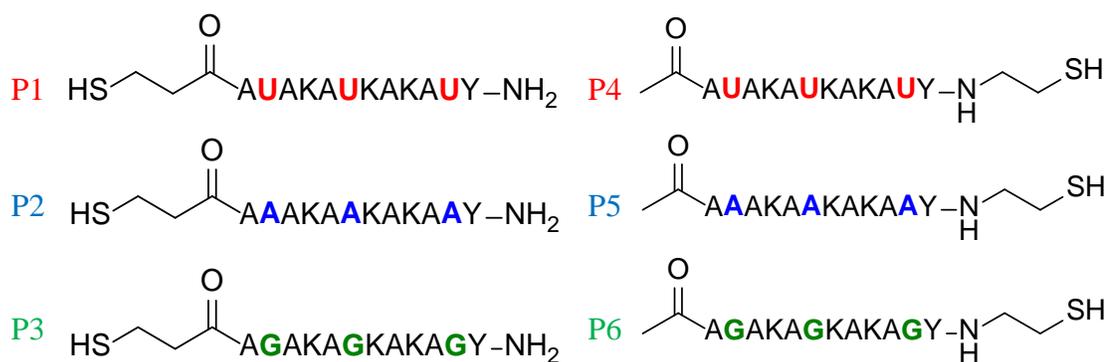
Figure 5.1. Two sets of α-peptide sequences for C- or N-terminus attachment to gold surface.

5.2   RESULTS AND DISCUSSION

5.2.1   Circular Dichroism and relative helicity.

Circular dichroism (CD) was used to estimate the relative helicity of each peptide studied. CD is a useful technique for the rapid assessment of helical and random-coil peptides

due to the unequal absorption of left- and right-handed circularly polarized light. CD allows for the determination of the secondary structure of peptides through the characteristic absorption peak locations for α-helix, anti-parallel β, and disordered structures as seen in Figure 5.2. With this information, it is possible to order the peptide sequences by the degree of helicity. Peptides 1 and 4 (AIB-substituted) are the most helical, while peptides 3 and 6 (glycine-substituted) are the least helical.
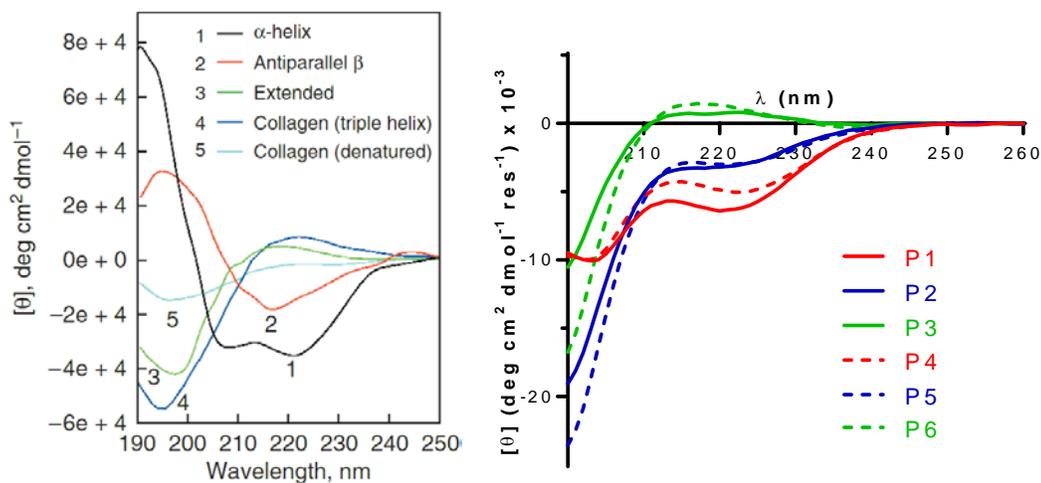
Figure 5.2. Left.) CD spectra of polypeptides with characteristic peak locations. Right.) CD spectra of peptides 1-3, and their inverses 4-6.

5.2.2 Fourier Transform Infrared Spectroscopy (FTIR) and Polarization Modulation Infrared Reflectance Absorption Spectroscopy (PMIRRAS).

Circular dichroism is an excellent technique for rapid assessment of the secondary peptide structure; however, this measurement can only be taken in solution. Since self-assembled monolayers are surface-bound, another technique is needed to determine their secondary structure. FTIR is a significantly more sensitive technique to secondary structure than CD, allowing for lower concentrations required for analysis. [82] Peptides have amide A & B and amide I-VII modes arising from in- and out- of plane displacements. Most of these modes are quite complex, but amide I and II are well understood. Amide I is the characteristic C=O and C-N stretching vibration, occurring around 1600-1700 cm^{-1}; amide II is the N-H bending and C-N stretching mode and occurs around 1500-1600 cm^{-1}. Increasing degrees of helicity cause this peak to become red-shifted, shown in Figure 5.3.
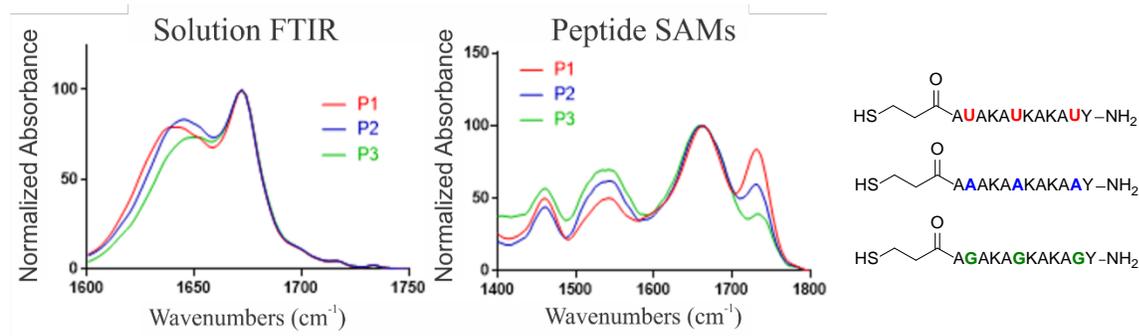
Figure 5.3. FTIR of α-peptides in solution and as monolayer.

Using FTIR, it is possible to determine the secondary structure of the peptide on the surface; however, background water is difficult to subtract from the scans due to the hydrophilicity of the peptides. Water can be displaced with D_2O in order to alleviate some of these issues, but the peaks become shifted and broader due to the exchange capabilities of deuterium.[83] D_2O does not absorb in the Amide I region and is relatively free from interference from water peaks.
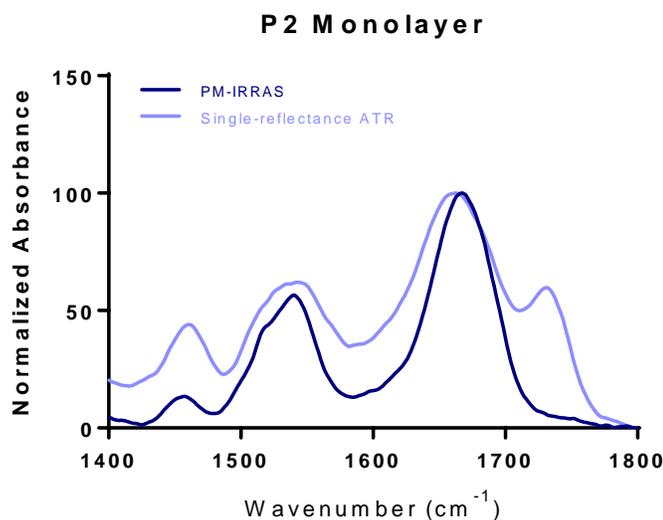
P2 Monolayer

Figure 5.4. Example monolayer structure assessment using FT-ATR and PM-IRRAS.

One downside to FTIR is that although the sensitivity to the monolayer is high, there is broadening that can occur hiding the peak shifts which are indicative of more- or less-helical α-peptides, Figure 5.4. A possible alternative is to use polarization modulation infrared reflectance absorption spectroscopy, PMIRRAS, instead of FT-ATR. This technique is insensitive to atmospheric H_2O and CO_2 and only molecular vibrations with some fraction of a dipole moment perpendicular to the surface are active. These PMIRRAS experiments will be performed shortly.

5.2.3 X-Ray Photoelectron Spectroscopy (XPS) for packing density determination.
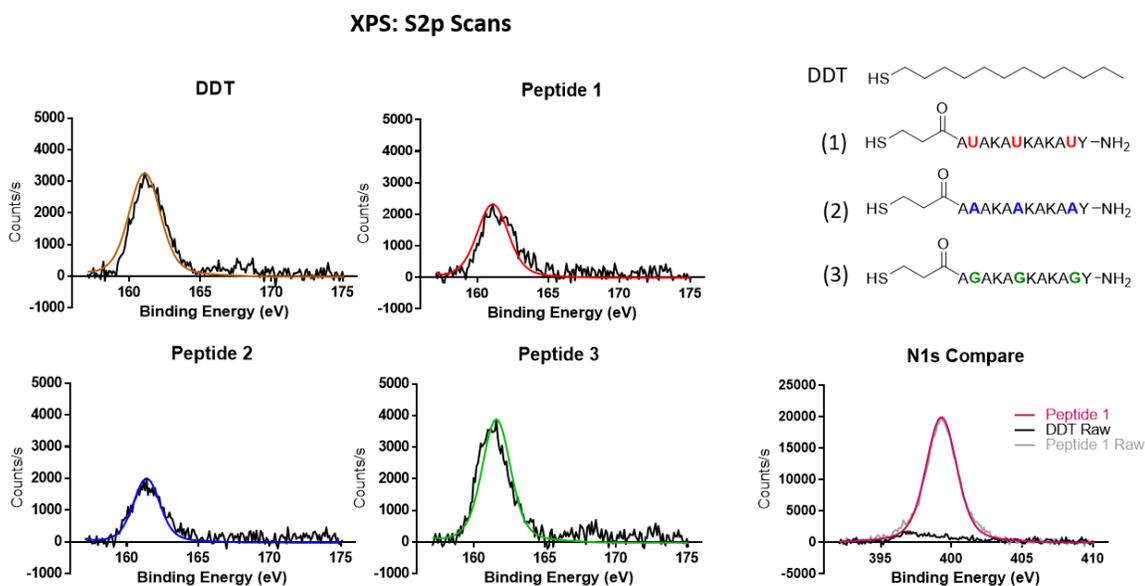
Figure 5.5. Left.) Sulfur 2p peaks for DDT and first series of peptides. Right.) Sequence and lack of N1s peak for DDT as expected.

An increased packing density of the peptide SAMs could lead to an increased piezoelectric response due to more molecules interacting with the tip, causing a larger deformation. With XPS, two goals can be achieved: the integrity of the sulfur-gold linkage can be confirmed and the packing density of the peptides on gold can be determined relative to a dodecanethiol standard.[84] The S2p peaks in Figure 5.5 are indicative of a gold-thiol interaction for a SAM, confirming the integrity of the bond.

To estimate the packing density, the ratio of sulfur-to-gold peak maxima of each peptide is compared to the packing density of DDT. The packing density for each peptide is comparable to that of DDT (4.62×10^{14} molecules per cm^2). The small variation of the packing density is not

enough to affect the piezoelectric response of the monolayers, nor is there any apparent trend between helicity of the peptide and packing density.
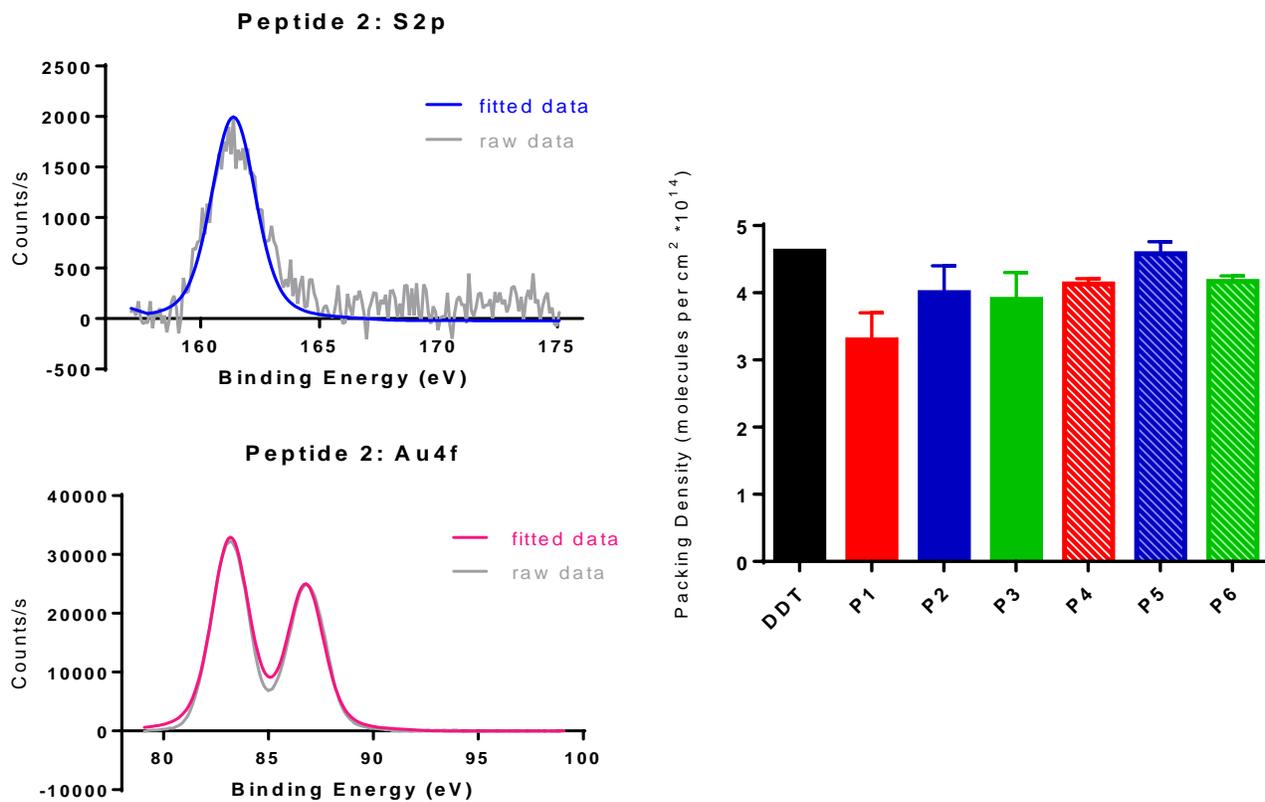
Figure 5.6. Left.) Sample XPS data for peptide 2. Right.) Average packing density for DDT and peptides 1-6.

5.2.4 Piezoelectric Force Microscopy (PFM) and Dual AC Resonance Tracking (DART).
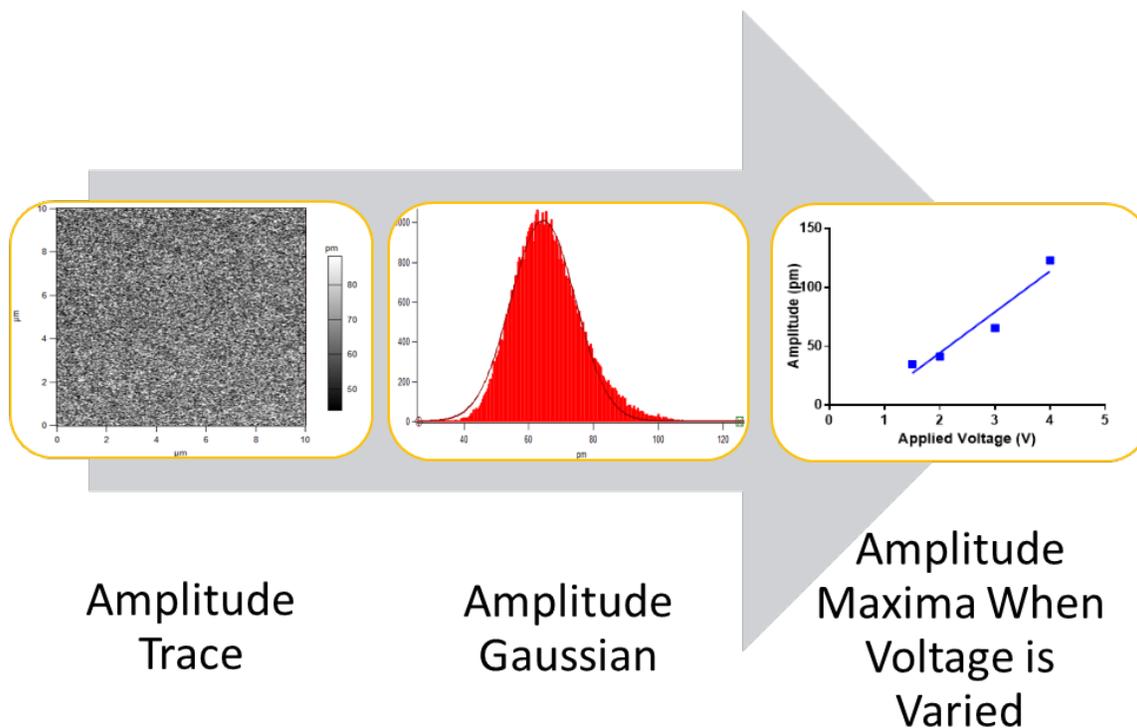
Figure 5.7. Process for acquiring semi-quantitative piezoresponse response of the peptides.

Measurement of the piezoelectric response of a self-assembled monolayer (SAM) is performed using an atomic force microscope (AFM) with the dual-AC resonance tracking-piezoresponse force microscopy technique (DART-PFM). The change in thickness, Δt, of the film is measured over a series of voltages ranging from 1.5 to 4 V as seen in Table 5.1. The resulting slope of the line is a close approximation to the piezoelectric response of these films. Ideally, the intercept of this line would pass through zero, however, due to electrostatic and tip-sample interactions that is rarely the case.

Table 5.1. Piezoelectric response data for peptides A-C, dodecanethiol (DDT), and quartz using DART-PFM.

Date	Sample	PFM Amplitude at				Piezo. Coefficient (pm V^{-1})	R^2
		1.5 V	2.0 V	3.0 V	4.0 V		
11/3/2016							
	Peptide A	0.30	0.39	0.53	0.68	0.15 ± .004	0.999
	Peptide B	0.28	0.35	0.44	0.69	0.16 ± 0.02	0.956
	Peptide C	0.24	0.37	0.49	0.63	0.16 ± 0.02	0.963
11/9/2016							
	Peptide A	2.06	2.55	3.34	4.36	0.90 ± 0.03	0.997
	Peptide C	3.10	3.36	5.17	6.56	1.45 ± 0.13	0.984
11/10/2016							
	Peptide A	2.61	3.14	6.32	9.83	2.80 ± 0.30	0.967
	Peptide B	2.72	3.09	5.92	8.69	2.47 ± 0.16	0.982
	Peptide C	2.67	2.81	6.14	9.94	2.90 ± 0.30	0.957
	DDT	1.47	1.90	2.45	3.44	0.76 ± .07	0.984
11/14/2016							
	Peptide A	5.17	8.59	11.01	11.02	2.20 ± 0.79	0.770
	Peptide B	1.68	2.33	3.02	4.34	1.02 ± 0.10	0.982
	Peptide C	2.55	2.83	4.76	6.74	1.74 ± 0.17	0.982
12/9/2016							
	Peptide A	1.45	2.10	2.31	3.76	0.84 ± 0.19	0.910
	Peptide B	1.94	3.75	7.00	7.87	2.42 ± 0.45	0.935
	Peptide C	1.79	2.02	3.40	4.05	0.97 ± 0.12	0.972
2/2/2017							
	Quartz	1.05	1.74	1.85	2.45	0.49 ± .13	0.883
	Quartz	4.13	5.79	8.39	11.50	2.90 ± 0.08	0.998
	Quartz	5.86	7.72	7.31	15.15	3.30 ± 1.28	0.768
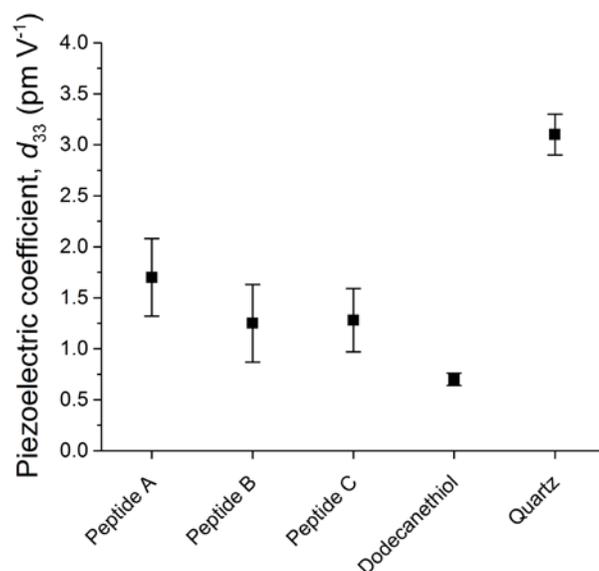
Figure 5.8. Piezoelectric response of peptides A-C with dodecanethiol and quartz as reference.

The average response of the peptides is significantly greater than the dodecanethiol monolayers. For the individual peptides, the average responses were 1.70 ± 0.38, 1.25 ± 0.38, and 1.28 ± 0.31 pm V^{-1} for peptide A, B, and C, respectively, and 0.70 ± 0.06 pm V^{-1} for dodecanethiol. Using our method, the piezoelectric response of quartz was found to be 3.10 ± 0.20 pm V^{-1}, close to the known value for d_{11} of 2.3 pm V^{-1}.[85] The d_{33} of these peptides is greater than the response of collagen (0.8 pm V^{-1}),[86] bone (0.29 pm V^{-1}),[87] and wood (0.04 pm V^{-1}).[88] Although these peptides do not exhibit a greater response than quartz, this research provides a foundation for future synthetic targets of peptidic piezomaterials.

5.3   CONCLUSIONS

The α-peptides that were used in this set of experiments exhibited the piezoelectric property when tested as SAMs on gold. However, exploring the hypothesis that there is a correlation between the helicity of an α-peptide did not lead to a confirmation of the hypothesis. The peptides did not exhibit significantly different piezoelectric responses; however, the responses were significantly greater than dodecanethiol, thus, showing promise for this novel class of piezoelectric materials. One future direction of this work is to pattern the surface with an internal standard of a non-piezoactive molecule, such as 1-dodecanethiol (DDT) which will allow for a more quantitative approach to the determination of d_{33} due to the relationship between the peptide and DDT's response. Second, expanding the library of piezoelectric molecules to include molecular foldamers[89] which are able to utilize the design rules elucidated in the computational work previously discussed,[81] a complete understanding of the piezoelectric effect of molecular monolayers can be had.

Further exploration of the origin and optimization of the piezoelectric property of materials moves this research into the bulk scale. Increased flexibility and dipole moment/polarizability have shown to have large influence on the response of single-molecules and SAMs; this information can be applied to the bulk scale by optimizing each component (flexibility and dipole moment) individually. The validity of the hypothesis can be tested by choosing a matrix to be doped with a polar molecule. A flexible matrix, such as polyurethane foam, doped with varied concentrations of polar molecules will provide the same conclusions that were found from the computational and experimental work on the small-molecule systems.

6.0   MOLECULARLY-DOPED POLYURETHANE FOAMS WITH MASSIVE PIEZOELECTRIC RESPONSE

This work, written in collaboration with Michael Moody and Geoffrey R. Hutchison*, was, in part, published as *J. Mat. Chem. C*, **2016**, 4 (20), 4387-4392. Copyright 2016, Royal Society of Chemistry.

The author performed experiments and assisted in the development of the mathematical explanation for the effect.

6.1   INTRODUCTION

Piezoelectric materials have many technological applications, from actuators and sensors to energy harvesting, and besides the commercialized ceramics and polymers, there are promising piezoelectrics from a variety of material classes such as ceramic and polymer composites,[90-92] space-charge electrets,[93] nanostructured ceramics,[94,95] and molecular monolayers.[81] Nonetheless, each category has particular weaknesses as well as particular strengths, and it may be that none of these is the optimal material class for piezoelectric performance. Ceramics such as lead zirconium titanate (PZT) are widely used and routinely have d_{33} piezocoefficients above 200 pC/N,[96] but they have limited flexibility. Polymers can be subjected to larger mechanical strains,[97] be formed more easily, and be poled at lower

temperatures, down to room temperature,[98] but their piezoresponse is at best an order of magnitude lower than PZT (e.g., for polyvinylidene difluoride (PVDF) 20-30 pC/N).[96] An interesting approach is demonstrated in the space-charge electrets, where corona poling a voided, nonpolar polymer causes charge accumulation.[99] These structured materials can outperform ceramics in both piezocoefficient (routinely from 200 to 800 pC/N)[100,101] flexibility, and although temporal and thermal stability remain weak points, improvements have been made.[102]

The developments in space-charge electrets indicate that successful piezomaterials need not be crystalline or have unit-cell-scale dipoles. In developing better piezoelectric materials, it is desirable to consider other types materials that have highly polar, deformable elements. While the figures of merit are different, polar nonlinear optical (NLO) materials have some similar demands and some insightful design schemes. For example, doping a nonpolar polymer with a polar compound has yielded considerable success, allowing the optimization of the dopant for ideal optical properties and the optimization of the polymer for easy processing.[103-105] Complex chromophore molecules are dispersed in nonpolar polymers such as poly(methyl methacrylate) (PMMA) and poled to produce axial alignment.

In this work, we use the design concept of doped nonpolar polymers to create a new type of flexible piezoelectric material. Here, the polarization and the bulk structure are provided by two different systems, so each can be optimized independently. Mechanical properties are largely determined by the host matrix, and so ideal mechanical properties, very important for usable piezomaterials, can be selected from a large set of commodity polymers while relying on the dopant molecules for electric polarization.

A dopant approach seems promising, but previous measurements of electromechanical response of NLO materials have shown piezocoefficients of 1-2.5 pC/N,[106,107] an order of

magnitude below PVDF. These materials, however, had been optimized for optical properties. A simple model can guide the way to improved piezoelectric properties.

Some analyses of piezoelectric properties of dipole-doped systems have been published, and accurate calculation requires careful treatment.[108,109] General design rules, however, can be obtained even from basic estimates.

The direct piezoelectric effect is the change in surface charge due to an applied force. This can be quantified by the d_{ij} piezoelectric tensor elements (or simply piezocoefficients), typically in pC/N. Because a polarization difference between two regions is equivalent to a surface charge on their boundary, the piezoelectric charge per unit force can also be expressed as the change in electric polarization (dipole moment density) per unit stress, and so the piezocoefficient can be rewritten as in Equation (6.1).

$$d = \frac{dQ}{F} = \frac{\frac{dQ}{A}}{\frac{F}{A}} = \frac{dP}{\sigma} \tag{6.1}$$

where P is electric polarization and σ is the stress. The macroscopic polarization can be related to the total molecular dipole moment (μ) of all dopant molecules with a correction for the dielectric constant given in Equation (6.2).[108]

$$P = \frac{\epsilon_\infty + 2}{3} * \frac{\mu}{V} \tag{6.2}$$

where μ is the net dipole moment, V is the volume, and ϵ_∞ is the dielectric constant in the absence of dipolar rearrangement (e.g. at frequencies above molecular rotations).

For the system considered here, the deformation of the dipoles should be small compared to the deformation of the bulk matrix. If the total dipole moment is assumed to be constant, the polarization change during compression is due only to the change in volume. Carrying out

derivatives with this assumption and rearranging gives Equation (6.3).

$$\frac{dP}{\sigma} = \frac{d\left(\frac{\epsilon_\infty+2}{3}*\frac{\mu}{V}\right)}{\sigma} = \frac{\epsilon_\infty+2}{3} * \frac{\frac{-\mu dV}{V^2}}{\sigma} = \frac{\epsilon_\infty+2}{3} * \frac{-\mu/V}{\frac{\sigma}{dV/V}} \qquad (6.3)$$

For uniaxial stress in the small strain limit, the volume change is given by Equation (6.4).

$$\frac{dV}{V} = (1-2v)\varepsilon = (1-2v)*\frac{\sigma}{E} \qquad (6.4)$$

where v is Poisson's ratio, ε is the strain, σ is the stress, and E is Young's modulus. Using Lamé's relation between Poisson's ratio, the bulk modulus K, and Young's modulus yields Equation (6.5).

$$\frac{dV}{V} = \left(1 - 2*\left(1/2 - \frac{E}{6K}\right)\right)\frac{\sigma}{E} = \frac{\sigma}{3K} \qquad (6.5)$$

Combining equations (6.3) and (6.5) gives Equation (6.6) as an estimate of the piezocoefficient:

$$d = \frac{\epsilon_0+2}{3} * \frac{-\mu/V}{3K} \qquad (6.6)$$

Values can be calculated for a typical chromophore-doped, poled polymer material. A reasonable value for ϵ_∞ may be 4 (see APPENDIX C). Since the poling is less than unity, the polarization should be scaled by approximately 0.3, typical for the poling fraction in NLO materials.[107] For a PMMA matrix (K = 6.1 GPa)[110] with a 1 M concentration of a dopant with a molecular dipole moment of 10 D, the expected piezocoefficient using Equation 6.3 is 0.7 pC/N, in reasonable agreement with reports of NLO materials with piezocoefficients up to 2.5 pC/N.[106,107] Despite the high polarizations achieved in these materials, the piezocoefficient is low, since the bulk modulus is too high.

In optimizing the piezoresponse, low bulk modulus as well as high polarization will contribute to a large piezocoefficient. Indeed, an inverse relationship between elastic stiffness

and piezocoefficient has been observed in space-charge electrets.[111] Even in conventional polymer piezomaterials such as PVDF, meso- and nanoporous samples yield higher output current than bulk samples,[112,113] which may be partly explained by this mechanism. Although assumptions were made in deriving the formula here, the qualitative relationship between d piezocoefficient and elastic modulus is general and can be useful as a design principal in many classes of materials.

Here, the drive for low modulus materials suggests the use of a structured material such as a foam, to achieve a bulk modulus orders of magnitude lower than other materials of similar composition. A foam structure results in decreased polarization because of the reduced relative density, but this will be offset by the favorable mechanical properties.

The theoretical bulk modulus for open-cell foams with tetrakaidecahedral cells[114] is given in Equation (6.7), where E is Young's modulus and R is the relative density. Expressing the total polarization as the product of the bulk polymer polarization and the volume fraction of polymer (relative density), the piezocoefficient can be expressed as in Equation (6.8):

$$K = \frac{ER}{9} \tag{6.7}$$

$$d = \frac{\epsilon_\infty + 2}{3} * \frac{p/V}{3K} = \frac{\epsilon_\infty + 2}{3} * \frac{(p_{bulk}R)/V}{3 * ER/9} = \frac{\epsilon_\infty + 2}{3} * 3 \frac{p_{bulk}/V}{E} \tag{6.8}$$

Again, using the reasonably conservative ϵ_∞ value of 4 and a poling fraction of 0.3, the response for a foam system can be estimated. Using values for polyurethane (E = 100 MPa) with 2-chloro-4-nitroaniline (CNA), a polar small molecule (dipole moment 7.7 D) at a 0.5 M concentration (1 molecule/ 3.3 nm^3) gives a predicted piezocoefficient of 140 pC/N, an order of magnitude larger than PVDF. Although this calculation is only an estimate, the exceptional piezoelectric response warrants experimental testing. In this work, we report piezoelectric

polymer foams based on a commercial polyurethane foam doped with polar small molecules and electrode-poled.

6.2   EXPERIMENTAL

Polytek Development Corporation PolyFoam F-3 polyurethane precursors (part A, Methylene bis(phenylisocyanate) and other isomers, and part B, polyether polyol and proprietary copolymer) were obtained from BITY Mold Supply. Dopants were dissolved either in polyurethane precursor part B or in acetone. Two parts precursor B and one part precursor A by mass were combined, with solvent if used, and mixed before being portioned into a poling fixture consisting of two electrodes (2 cm by 2 cm) with a fixed separation of 5 mm. Samples were cured for two hours at room temperature with an applied bias of up to 2 kV, and copper tape electrodes were attached to the top and bottom surfaces of the samples.

It was observed that increased ambient humidity affected results, so during periods of ambient humidity over 40%, precursors were mixed and poled in a glove bag with nitrogen fill (RH < 22%) and measured and stored in ambient conditions.

The quasistatic d_{33} piezocoefficient was measured with a screw-thread compression fixture and resistive force sensor (see schematic in Figure 6.1a) Short-circuit current from the sample electrodes and force sensor measurements were recorded with a Keithly 2612 sourcemeter while varying forces were applied manually with the fixture. Measured currents were integrated to determine charge, and the d_{33} piezocoefficient was calculated as the regression slope of charge

vs. force (as in Fig. 1b). Measurements were validated with commercial PVDF samples, which gave a d_{33} response of 27.3 ± 4.0 pC/N, in excellent agreement with the reported value.[96]
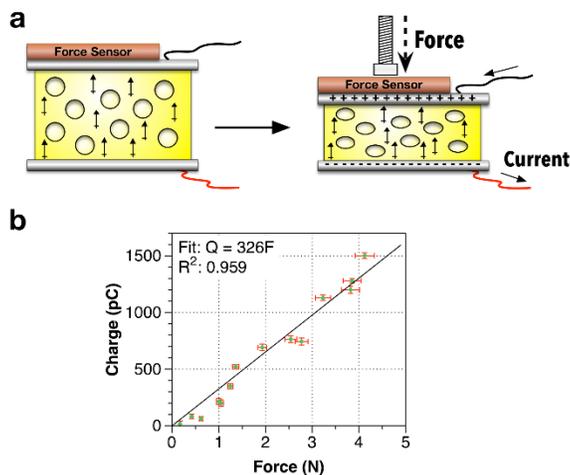
Figure 6.1. a) Schematic of foam material b) Net charge transferred as a function of applied force.

6.3   RESULTS AND DISCUSSION

In the model given by Equation (6.5), the piezocoefficient is directly proportional to the molecular dipole moment and the concentration of the dopant, but inversely proportional to the Young's modulus of the matrix, suggesting that an ideal system consists of a compliant polymer and a very polar dopant with a high solubility in the matrix and its precursors.

Testing of several dopants and poling conditions yielded foams in which electrical current was associated with the application of force such that the integrated current signal (charge) was proportional to applied force (e.g. as in Figure 6.1b). The slope of this relation is the direct effect piezocoefficient. (See APPENDIX C) Differences between various samples and unpoled or undoped controls indicated material piezoresponse as opposed to measurement-related noise.

69

Samples with varying concentrations of several dopants poled at 40 V mm^{-1} showed varying piezocoefficients, plotted in Figure 6.2 as a universal function of the product of dopant concentration and molecular dipole moment (the theoretical maximum polarization).

As expected, the piezocoefficient is proportional to the product of the concentration and the molecular dipole moment of the dopants. The response depends on the dipole moment but not other chemical or structural factors. Pure benzoic acid and CNA crystals are not inherently piezoelectric because they form centrosymmetric lattices (see APPENDIX C), yet their single-molecule polarity can be used by incorporating them as dopant molecules in a polymer matrix to create long-range polar order.

Quantitatively, the experimental piezoresponse of these samples is lower than the original calculation. Assuming a polyurethane Young's modulus of 100 MPa and converting to the units used experimentally, the predicted value of the slope in Figure 6.2 would be 121 pC/N D^{-1} M^{-1}. Thus, the measured response is only 5% of the value predicted for complete poling.
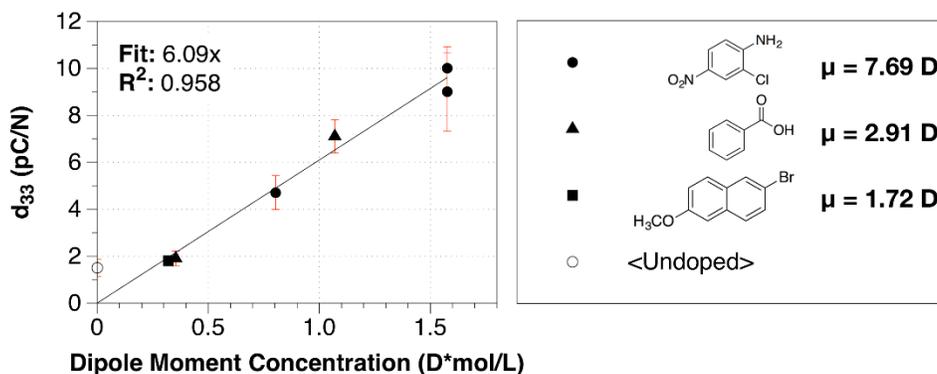
Figure 6.2. Piezocoefficient as a function of the product of dopant dipole and concentration when poled at 40 V mm^{-1}.

If the molecules are treated as independent dipoles in a uniform electric field, the equilibrium total polarization at a finite temperature T can be described by the Langevin function, Equation (6.9).[28]

$$P = \frac{N\mu}{V} * \left(\coth \frac{\mu E_{local}}{k_B T} - \frac{k_B T}{\mu E_{local}} \right) \tag{6.9}$$

where N/V is the concentration, μ is the molecular dipole moment, and k_B is Boltzmann's constant. E_{local} is the local electric field, for which varying values can be calculated depending on choice of model. Regardless of model, it is proportional to the applied field, and for small arguments, the Langevin function can be approximated as in Equation (6.10).

$$\frac{N\mu}{V} * \frac{\mu E_{local}}{3k_B T} \tag{6.10}$$

Thus, the polarization should be directly proportional to the poling field for weak fields.

In correspondence with this model, the piezocoefficient was observed to increase with poling field, as plotted in Figure 6.3. A response of 244 ± 30 pC/N was measured at the maximum poling field of 400 V mm^{-1}. This dramatically increased piezoelectric response indicates appreciable poling of the dissolved CNA molecules. Given that the original calculation uses an estimated dielectric constant and mechanical properties taken from specifications, this piezocoefficient is in good agreement with the model, which suggests the validity of the underlying mechanism.
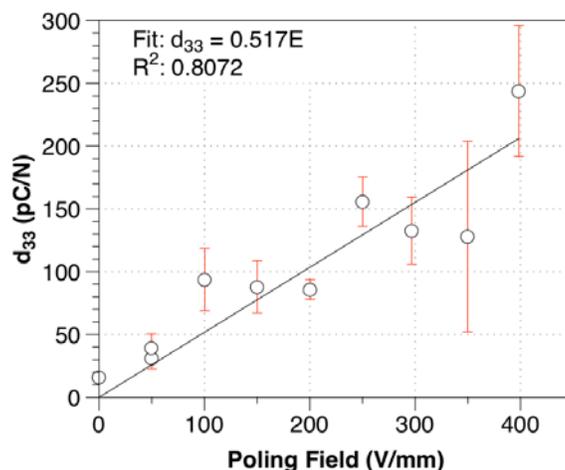
Figure 6.3. Piezocoefficient as a function of poling field for samples doped with 0.2 M 2-chloro-4-nitroaniline.

The voltage dependence distinguishes this effect experimentally from the mechanism in space-charge electrets. While the piezocoefficients of charged void systems also increase with poling field (as controlled by gas parameters in corona poling), the electric fields required for similar piezoelectric responses are two orders of magnitude higher.[11] The poling fields used here are well below the breakdown field of air, so the piezoelectric response here is unrelated to ionization and surface charge accumulation effects. These fields are also much lower than those necessary for electrostrictive-induced piezoelectric-like behavior, where piezoelectric behavior is only observed while applying large DC biases.[29]

We find that another poling-dependent property of these materials is stability. (Fig. S3 (APPENDIX C) shows the initial decay rate of samples versus poling field and stability over time.) Samples poled at low fields have responses which decay on the order of tens of minutes. Samples poled at fields of 150 V mm^{-1} or greater decrease by less than 20% over several days (over four days in some cases) and then decrease by over 80% in less than two days. In light of the significant poling fractions at these fields, the additional stability at higher poling fractions

may be conferred by a cooperative effect, and this stabilization may be lost once the poling fraction decreases below some threshold. At a concentration of 0.2 M, the average separation between solute molecules is 2.0 nm, slightly over three molecule lengths in the case of CNA, so dopant-dopant interactions are likely. Based on one model, dopant-dopant interactions increase sharply at scales below 1 nm.[30]

The mechanism of piezocoefficient decrease over time is hypothesized to be rotational diffusion of the dopants leading to depolarization, as has been observed in NLO materials.[19] Re-poling old, decayed samples over extended time periods (several days at room temperature) restored the response, up to 114% of the original response. This reversibility is consistent with flipping or conformational changes (i.e., molecular rotation in the polymer matrix) and seems to rule out chemical changes or physical degradation. Because the dopants are relatively small molecules without strong interactions with the polymer matrix, rotational diffusion at this rate is likely.[19] Larger dopants would likely improve stability by decreasing the rotational diffusion, as would increasing interaction with the matrix by crosslinking dopants into the polymer.[31] These approaches would likely have reduced solubility and added complexity, respectively.

As a further demonstration of the utility of this work, measurements of power output were made. A sample with a piezocoefficient of 112 pC/N had a voltage output of 307 mV/N at a frequency of 3 Hz, implying an impedance of 915 MΩ. The sample was connected to a load of 1 GΩ and subjected to light finger taps while current through the load and voltage across the load was measured. Typical finger taps yielded a peak current output of 5 nA and a peak power of 5 nW, with the power output varying with tapping intensity. Fig. 4a shows the power as a function of time and Fig. 4b shows the device, emphasizing the high flexibility.

Polyurethane foams are often used as shoe insoles, so one possible application would be self-powered sensors. If used in shoe inserts, this material would permit useful power output. Walking or running can produce over twice the body weight in instantaneous applied force. For a piezocoefficient of 250 pC/N, a loading of 1000 N once per second would yield an average current of 500 nA and peak currents above 5 μA. For an element ~15 cm^2 with a voltage output of 130 mV/N, this would mean an output power of 65 μW, or 43 mW/m^2. This is enough to power a low-power application specific integrated circuit (8 μW),[32] or, taking advantage of low-power sleep modes, a general purpose microcontroller with a low duty cycle. Multiple-layer devices could further increase power output and lower source impedance for ease of use with typical loads.

As this is a new approach, there are many avenues for further research. Demonstrating materials with higher stability by varying dopants would be desirable. Considering mechanical properties and changing the matrix could lead not only to higher piezocoefficients but also to materials tailored to specific applications. As this material system is a very general design, foams could be selected for high loss (active dampening) or low loss (energy harvesting). Changing the relative density should yield foams with the same piezocoefficient but a range of bulk moduli. The wide range of potential polymers and dopants may also allow selection for properties such as biodegradability[33] for transient implantable electronics,[34] or high optical transparency, impossible with current synthetic piezomaterials. In fact, unlike in space-charge electret materials, in this system the foam structure is not a key component of the electric polarization. Instead, the foam simply provides desirable mechanical properties. This approach could be applied to other materials with exceptionally low bulk moduli, such as brush polymers.[35] For a

given bulk modulus, non-porous materials are attractive because the polarization scales with the volume fraction of solid.

This range of opportunities stands in contrast to the slow pace of development of traditional piezoelectric materials and the modest pace of development of space-charge electrets. Though innovative work has improved poling fractions and processability of polymers such as PVDF, improvement is limited by the intrinsic piezocoefficient of the bulk polymer. In fact, the high k coupling constants that have been achieved are indicators of how little room remains for performance increases. Drastically increasing the piezocoefficient of a material with good efficiency (such as PZT, $k_{33} = 67\%$[36]) requires drastically changing other properties to satisfy conservation of energy. The general coupling efficiency is given in Equation (6.11).[36]

$$k = d\sqrt{\frac{Y}{\epsilon}}$$ (6.11)

Observing that the coupling efficiency cannot be greater than unity, the maximum d piezocoefficient is given by Equation (6.12).

$$d < \sqrt{\frac{\epsilon}{Y}}$$ (6.12)

The only ways to increase this limit on piezoresponse are to increase the dielectric constant or decrease the Young's modulus, and achieving large changes in either of these values for a conventional ceramic is not easy. For a polymer foam with a Young's modulus of 560 kPa and a dielectric constant of 4, this upper bound is already quite high, 8,000 pC/N, and it could be increased even further by decreasing the Young's modulus of the foam.

The coupling constant argument may be restated in simple mechanical terms. The amount of energy that can be harvested from a constant force increases with the amount of energy mechanically coupled into the material, which increases with decreasing Young's modulus. This

is not often addressed in bulk ceramic or polymer piezomaterial development, where it is difficult to tune mechanical properties over any large range. Ultimately, higher piezocoefficients can only be achieved by increasing the unity-efficiency limit, and the tunability of molecularly-doped polymer structures uniquely positions them to do so.

7.0   CONCLUSIONS

7.1   SUMMARY AND CONCLUSIONS

The goal of this research was to discover viable alternatives to conventional ceramic piezoelectric materials and devices via computational and experimental means.

Using density functional theory and Gaussian09, the origin of the piezoelectric effect in single molecules was explored. A computational method for the determination of the influence of regiochemistry, functional groups, dipole moment, polarizability, and steric effects on the piezoelectric response of these molecules was developed and two asymmetrically-substituted molecular spring scaffolds were proposed: [6]helicene and phenanthrene. The highly conjugated, rigid, structure of these backbones is analogous to the crystal structure of conventional piezoelectric materials, leading to the conclusion that the deformation of these molecular scaffolds is from the applied electric field, more than thermal influence. In addition, heteroatom substitutions to the backbone were made and the effect that the electron-rich and electron-poor qualities of these heterocycles had on the piezoresponse was examined. The computed piezoelectric responses of these materials are shown to be upwards of 110 pm V^{-1} for azahelicenes and 270 pm V^{-1} for "clamphene" molecules, or extended helicenes. The piezoelectric responses for these helicenes are on the same order of magnitude as PVDF and within the range of PZT.

Using the information gathered from the computational studies, a set of peptides with varying degrees of helicity was synthesized and the piezoelectric response of the peptide self-assembled monolayers was characterized using dual-AC resonance tracking piezoresponse force microscopy; an atomic force microscope technique. Through this semi-quantitative method, we show that the piezoelectric response of these peptide monolayers is within an order of magnitude to quartz, and significantly greater than non-piezoactive molecules such as 12-dodecanethiol. By doubling the length of the peptide, but keeping the sequence constant, no significant increase of the piezoelectric response was noted. These SAMs are advantageous since they provide a comparable response to quartz, with only a single-molecule film. These films provide a potential starting point for novel piezoelectric materials which take advantage of the ultra-thin, lightweight, tailorable qualities of organic and peptidic energy harvesting materials.

Expanding the piezoelectric research into the macroscale, we developed a novel class of piezoelectric material which is a composite foam device. In this material, we doped polyurethane foam with a polar organic molecule and aligned the dipoles in a process termed "poling." Neither of the component materials exhibited the piezoelectric effect even after poling; however, the composite material showed a significant electrical response. We showed that the piezoelectric response of these polyurethane foams is dependent on both the magnitude of the individual molecular dipole moment (different polar molecules) and the degree of alignment of the dipoles in the foam (varying poling voltages). The maximum response recorded from our piezoelectric foams was 244 pC N^{-1}, within the order of magnitude of PZT. With this material, we determined that the piezoelectric coefficient is proportional to the ratio of the dielectric constant of the material over the Young's modulus; i.e., the more polar, and more flexible the material, the greater the piezoelectric response.

7.2   FUTURE DIRECTIONS

There are several directions that this research can take beyond the results that are stated in this thesis. For the computational, analytical, and device aspect of this work, the future of this research is vast.

For the computational work in this thesis, a rapid, systematic approach to screening of potential synthetic targets using the [6]helicene backbone would be useful for the advancement of understanding to include the spring constant in the direction of deformation. This approach could utilize a genetic algorithm to design novel piezoelectric helicene derivatives with a faster throughput of variation from what was screened in this thesis work. Variations can include functional group substitutions along the backbone, a larger range of heteroatoms, or extended helicene systems.

Even though these piezoelectric materials have large computed piezoresponses, the synthetic accessibility of the asymmetrically-substituted [6]helicenes is rather low. A novel synthetic route is required to create the [6]helicene derivatives with significant yield. Typical approaches involve synthesis beginning at one functional group and building the helicene from that point.[115] While this is effective for some molecules, the yield of this approach is very small in practice. A potentially successful approach would be to begin with a naphthalene derivative and build the helicene from there, as shown in Figure 7.1. There is a synthetic by-product of the first coupling reaction where the 2-aminostyrene adds to both sides of the naphthalene forming the symmetric product. This by-product can be avoided by adding a 1:1 equivalency.
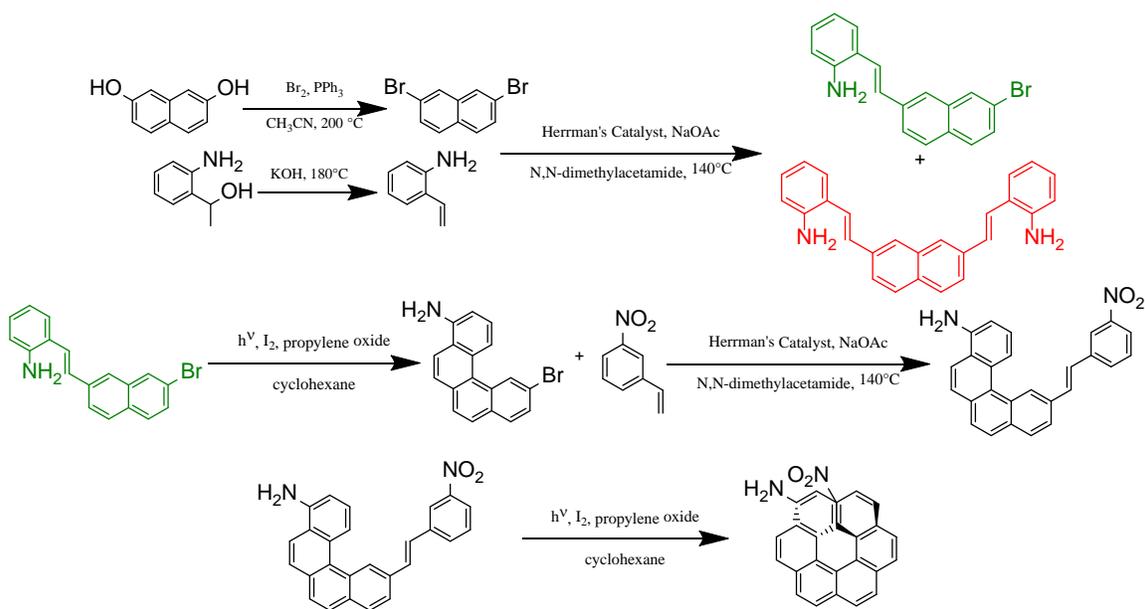
Figure 7.1. Potential synthetic scheme for the synthesis of asymmetrically substituted [6]helicene.

The piezoelectric response of the peptides has plenty of room for improvement. With a piezoelectric response on the order of magnitude of quartz (~2.5 pm V^{-1}), the response is on the

low side for comparable materials. Moving forward with the piezoelectric peptides will involve increasing the charge density and the flexibility of the backbone of the system. The charge density can be increased with charged side groups such as lysine or glutamate. As for the flexibility, short alkane side chains, such as glycine, can be added into the sequence. Preliminary computational studies show that these responses should also be similar to the [6]helicenes of ~100 pm V^{-1}.

APPENDIX A

SYNTHESIS OF ASYMMETRIC [6]HELICENES

This appendix discusses the attempts at synthesis of the asymmetric [6]helicene molecules discovered to exhibit high computed piezoelectric responses. The NMR spectra for the compounds can be found in appendix B.

A.1   SYNTHETIC METHODS

2-Bromo-6-methoxynaphthalene (97%), 3-bromostyrene (97%), 3-vinylbenzoic acid (97%), sodium acetate, and potassium hydroxide were purchased from Fisher/Acros. 4-Bromostyrene (98%), *N*,*N*-dimethylacetamide, 2-aminophenethyl alcohol (97%), and (±)propylene oxide (98%) were purchased from Aldrich Chemical Co., Inc. Hermann-Beller's catalyst (trans-di(μ-aceto)bis[o-di-o-tolylphosphino)benzyl]dipalladium(II), 97+%) was purchased from Strem Chemicals, Inc. 2,7-Dibromonaphthalene was purchased from TCI America. All chemicals were used as received without further purification.

Argon (grade 4.8) was supplied by Matheson TriGas. The photo-reactor is self-designed and fabricated from the university glass shop. UV light source is from Philips (319657 H39kb-175 Mercury Vapor Lamps, 175W, with outer glass shell removed by the university glass shop). Electronic ballast is allocated from the university electronic shop.

NMR measurements were performed on a Bruker 300 or 400 Ultrashield™ magnets with AVANCE III 300 or 400 Console (Bruker Biospin, Billerica, MA). Gas chromatograph-mass spectrometer (GC-MS) measurements were taken on a Shimadzu GCMS-QP2010S fitted with an AOC-20i autoinjector.
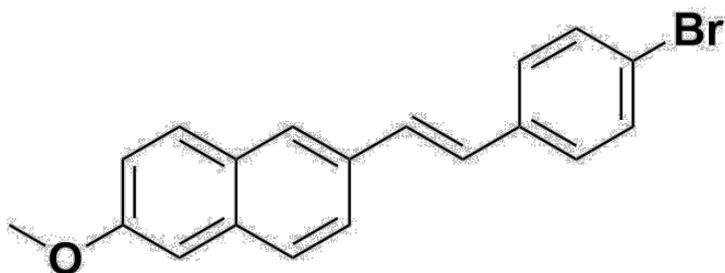
Appendix Figure 1. 2-(4-bromostyryl)-6-methoxynaphthalene

To a mixture of 2-bromo-6-methyoxynaphthalene (2.37 g, 10.00 mmol) and 4-bromostyrene (2.00 mL, 14.00 mmol) in *N,N*-dimethylacetamide (50 mL) in a two-neck round bottom flask charged with a stir bar, was added sodium acetate (0.902 g, 11.00 mmol) and *trans*-bis(acetato)bis[o-(di-o-tolylphosphino)benzyl]dipalladium(II) (140.6 mg, 0.150 mmol) under nitrogen and was heated to 130 °C. After stirring at 130 ºC for 48 hr, the reaction mixture was cooled to room temperature and quenched with 5% HCl solution and the aqueous layer was extracted with dichloromethane. The combined organic layers were washed with brine, dried over magnesium sulfate, filtered, and concentrated under reduced pressure. The crude product was purified by column chromatography (10% ethyl acetate in cyclohexane) to afford2-(4-bromostyryl)-6-ethoxynaphthalene (18.0 mg, 0.0531 mmol, 0.53% recovery) as a light yellow solid. ^{1}H NMR (400 MHz, CDCl3): δ 3.933 (s, 3H), 7.127 (t, J = 12 Hz, 3H), 7.164 (s, 1H),

7.209 (s, 1H), 7.251 (s, 1H), 7.45 (dd, J = 16.4, 8.4 Hz, 4H), 7.715 (m, 3H), 7.789 (s, 1H).; ^{13}C NMR (400 MHz, CDCl3): δ 158.08, 131.94, 127.77, 129.74, 129.71, 128.02, 127.40, 126.84, 126.82, 124.13, 119.29, 106.09, 55.50; GC-MS for $C_{19}H_{15}BrO$ ([M+]): 338.
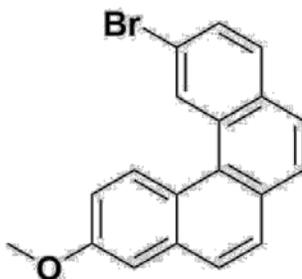
Appendix Figure 2. 2-bromo-10-methoxybenzo[*c*]phenanthrene

To a solution of 2-(4-bromostyryl)-6-methoxynaphthalene (18.0 mg, 0.0531 mmol) in cyclohexane (100 mL) was added iodine (13.5 mg, 0.0531 mmol) and propylene oxide (0.308 g, 0.372 mL, 5.31 mmol) under inert atmosphere. The reaction mixture was irradiated using a 175 W Hg-lamp. After 4 h of irradiation and stirring, the reaction mixture was concentrated under reduced pressure and yielded 2-bromo-10-methoxybenzo[*c*]phenanthrene as a light yellow-green solid. ^{1}H-NMR (300 MHz; CDCl$_3$): δ 3.47 (s, 3H), 6.72 (s, 1H), 6.83 (s, 1H), 6.85 (t, J= 3.5 Hz, 1H), 7.15 (dd, J= 8.5, 1.7 Hz, 1H), 7.23 (s, 1H), 7.29 (s, 1H), 7.31 (s, 1H), 7.34 (s, 1H), 8.38 (s, 1H), 8.66 (s, 1H); GC-MS for $C_{19}H_{13}BrO$ ([M+]): m/z = 336.
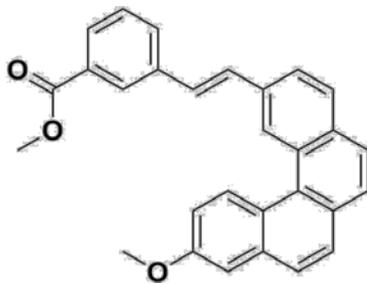
Appendix Figure 3. Methyl 3-(2-(10-methoxybenzo[*c*]phenanthrene-2-yl)vinyl) benzoate

To a mixture of 2-bromo-10-methoxybenzo[c]phenanthrene (13.0 mg, 0.039 mmol) and methyl 3-vinylbenzoate (0.1 mL, 0.652 mmol) in *N,N*-dimethylacetamide (20 mL) in a two-neck round bottom flask charged with astir bar, was added sodium acetate (3.20 mg, 0.039 mmol) and *trans*-bis(acetato)bis[o-(di-o-tolylphosphino)benzyl]dipalladium(II) (2.00 mg, 0.002 mmol) under nitrogen and was heated to 130 ℃. After stirring at 130 ℃ for 24 hr, the reaction mixture was cooled to room temperature and quenched with 5% HCl solution and the aqueous layer was extracted with dichloromethane. The combined organic layers were washed with brine, dried over magnesium sulfate, filtered, and concentrated under reduced pressure. The crude product was purified by column chromatography (10% ethyl acetate in cyclohexane) to afford methyl 3-(2-(10-methoxybenzo[c]phenanthren-2-yl)vinyl) benzoate(9.2 mg, 0.0220 mmol, 57% yield) as a light yellow solid.

Appendix Figure 4. 2-vinylaniline

2-Amino-phenethylalcohol (2.08 g, 15.1 mmol) and potassium hydroxide (1.10g, 19.6mmol) were combined in a distillation apparatus, then heated to 180 °C under vacuum. A clear, colorless oil was distilled over 3hours at 55 -60 °C at 0.25 Torr, 0.895g, 7.51 mmol, 50% yield.1H-NMR (300 MHz; CDCl3): δ 3.70 (s, 2H), 5.36 (dd, J= 11.0, 1.5 Hz, 1H), 5.68 (dd, J= 17.4, 1.5 Hz, 1H), 6.71 (dd, J= 8.0, 0.9 Hz, 1H), 6.86-6.77 (m, 2H), 7.14 (td, J= 7.6, 1.3 Hz, 1H), 7.35 (dd, J= 7.6, 1.4 Hz, 1H).
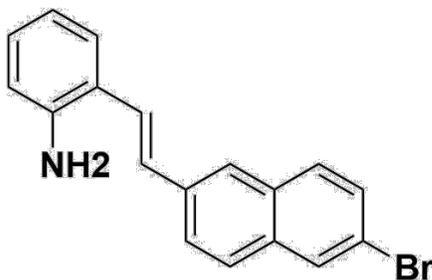
Appendix Figure 5. 2-(2-(7-bromonaphthalen-2-yl)vinyl)aniline

To a mixture of 2,7-dibromonaphthalene (1.00 g, 3.50 mmol) and 2-vinylaniline (0.417 g,0.824 mL, 3.50 mmol) in *N,N*-dimethylacetamide (25 mL) in a two-neck round bottom flask

charged with astir bar, was added sodium acetate (0.292 g, 3.85 mmol) and trans-bis(acetato)bis[o-(di-o-tolylphosphino)benzyl]dipalladium(II) (0.132 g, 0.141 mmol) under nitrogen and was heated to 130 ºC. After stirring at 130 ºC for 48 hr, the reaction mixture was cooled to room temperature and quenched with 5% HCl solution and the aqueous layer was extracted with dichloromethane. The combined organic layers were washed with brine, dried over magnesium sulfate, filtered, and concentrated under reduced pressure. The crude product was purified by column chromatography (10% ethyl acetate in hexanes) to afford (Z)-2-(2-(7-bromonaphthalen-2-yl) vinyl) aniline (97.0 mg, 0.299 mmol, 8.5% recovered) as a dark solid. GC-MS for $C_{18}H_{14}BrN$ ([M+]): m/z = 323.

APPENDIX B

NMR SPECTRA FOR [6]HELICENE SYNTHESIS

Over the next few pages, the NMR spectra for the [6]helicene synthesis will be presented.
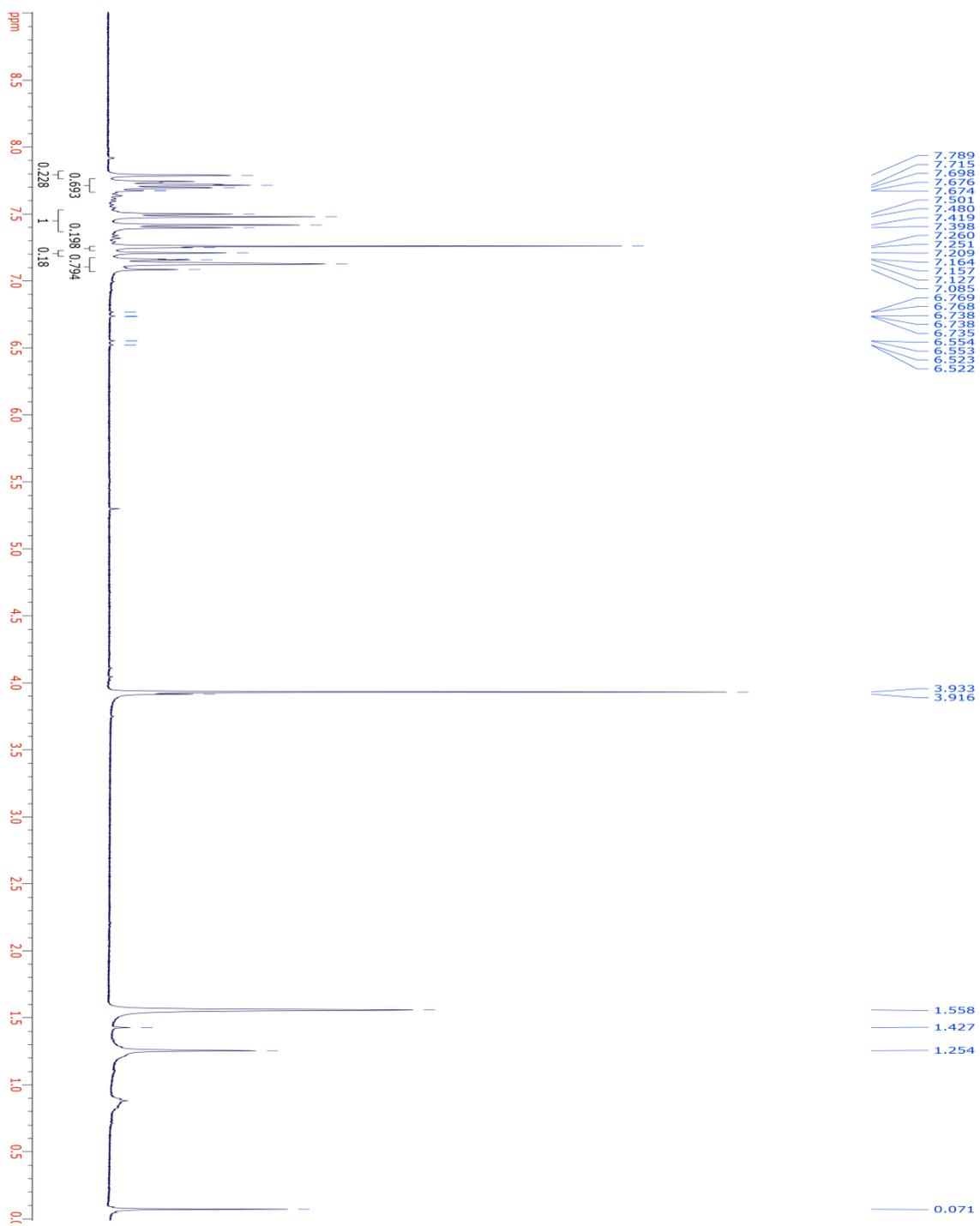
Appendix Figure 6. NMR of 2-(4-bromostyryl)-6-methoxynaphthalene, 400 MHz
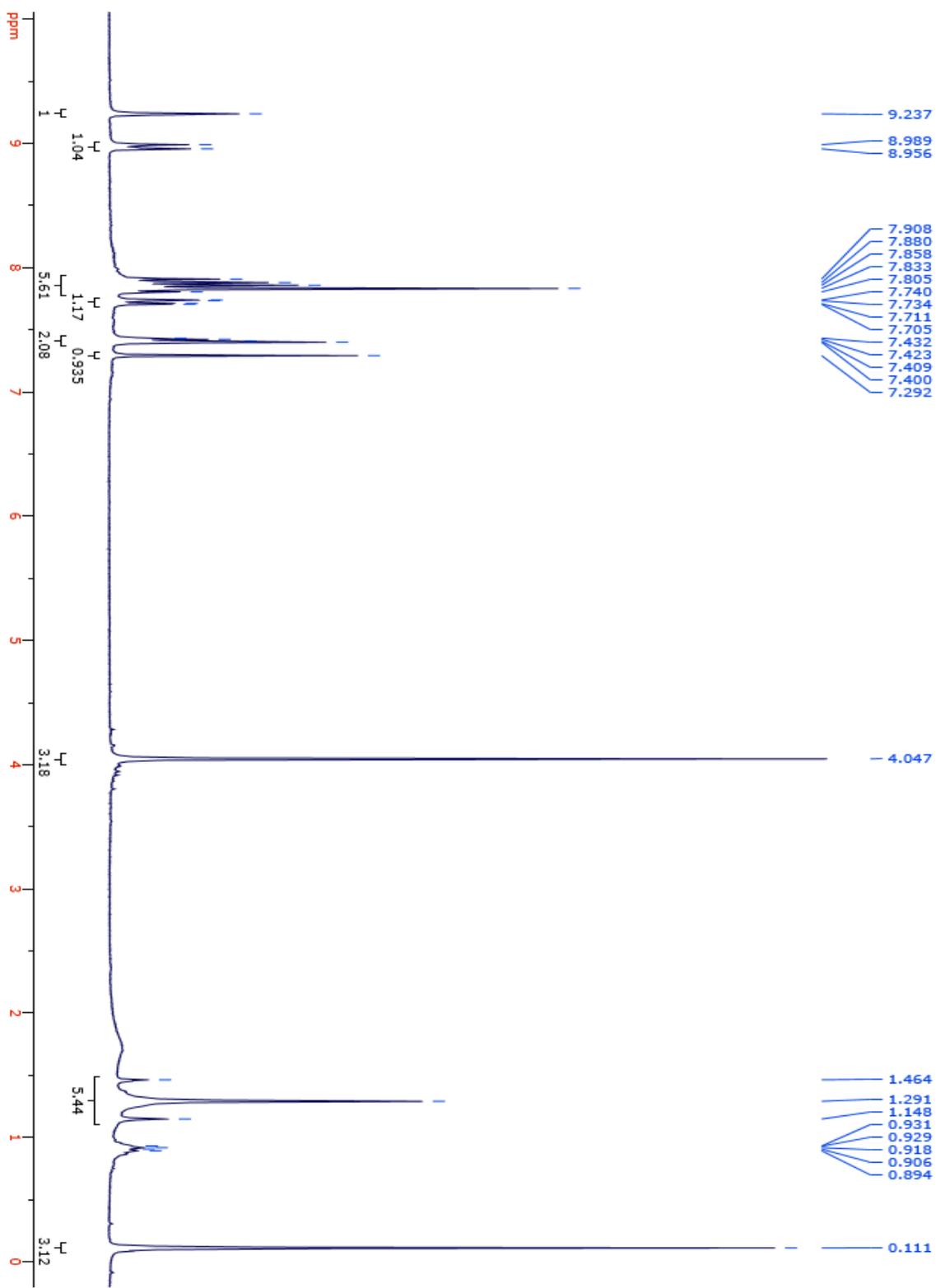
Appendix Figure 7. NMR of 2-bromo-10-methoxybenzo[*c*]phenanthrene, 400 MHz
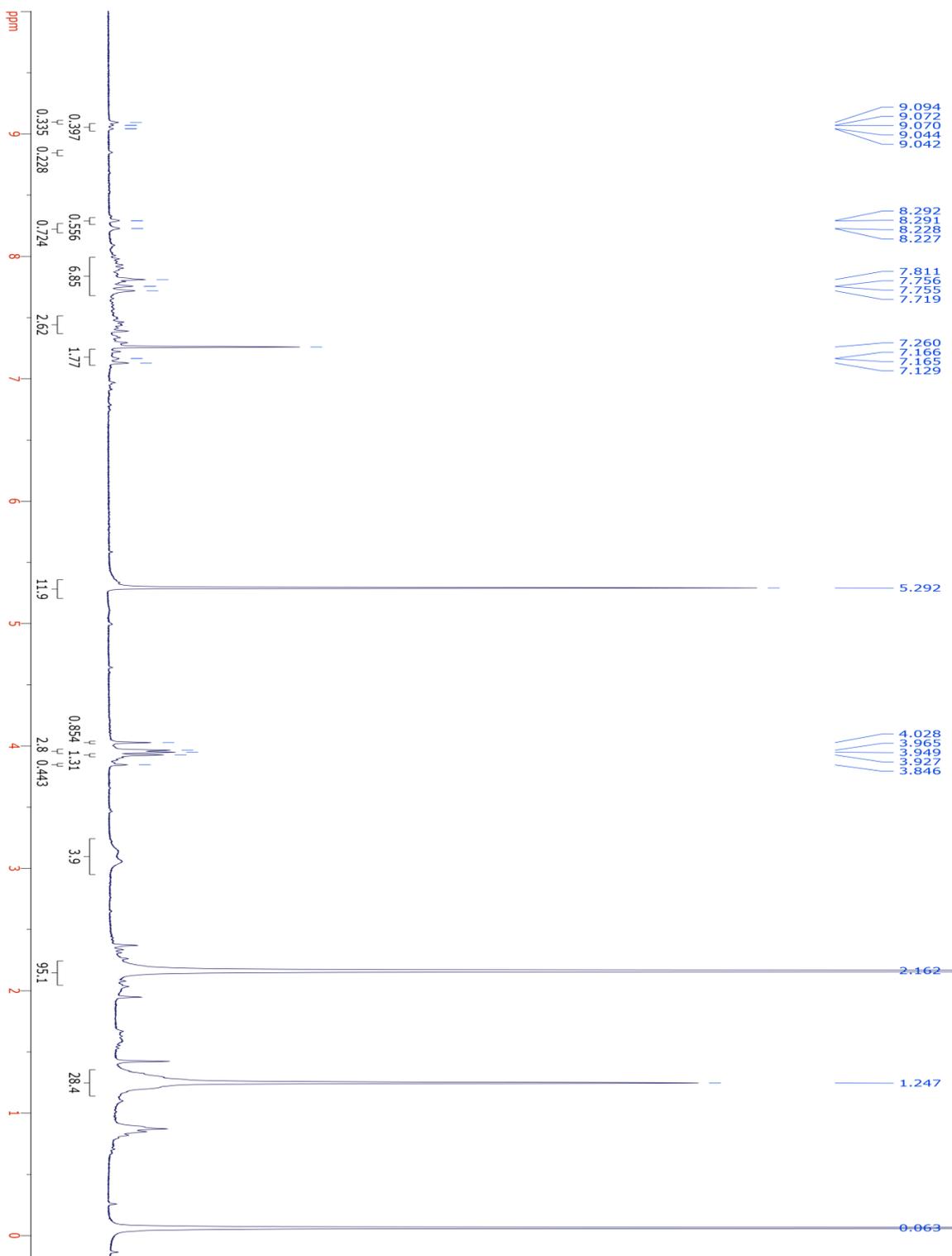
Appendix Figure 8. NMR of Methyl-3-(2-(10-methoxybenzo[*c*]phenanthrene-2-yl)vinyl) benzoate, 300 MHz
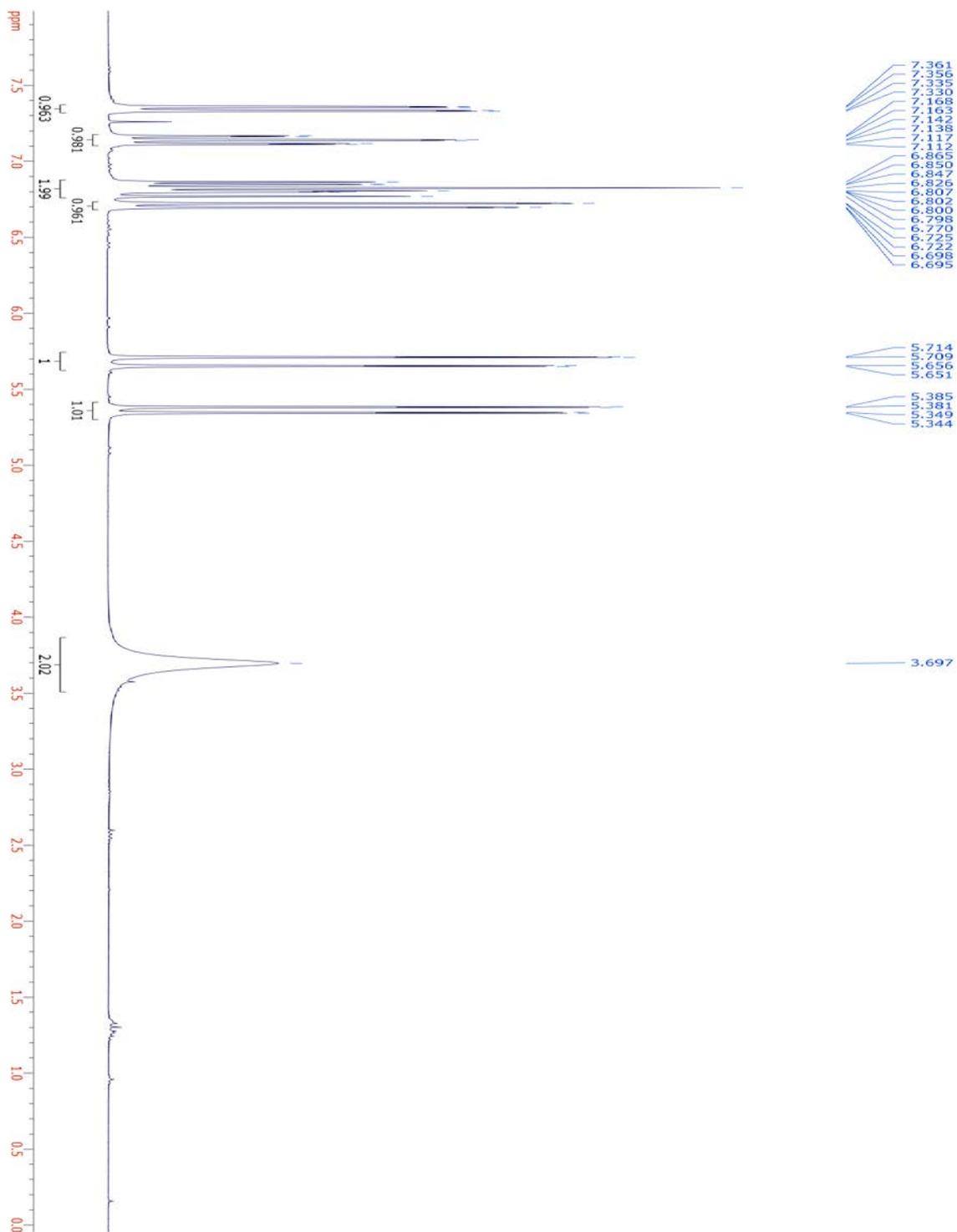
Appendix Figure 9. NMR of 2-aminostyrene, 400 MHz

APPENDIX C

SUPPORTING INFORMATION FOR PIEZOELECTRIC FOAMS

A.2   MEASUREMENT DETAILS

For measurement of quasistatic piezocoefficient, the sample electrodes were connected to one channel of a Keithly 2612 sourcemeter in ammeter configuration. A Tekscan Flexiforce A2013 resistive force was connected to another channel. A 1 V bias was applied to the Flexiforce sensor and the current was measured to calculate resistance. The force sensor has a reciprocal relation between applied force and resistance and had been previously calibrated with loads from 1 N to 60 N. The force sensor, electromagnetically shielded from the sample with copper tape, was placed over the sample in a stack consisting of a glass slide, the sample, another glass slide, the force sensor, and a PDMS spacer, and this was placed into a fixture consisting of a plastic contact point on a leadscrew operated manually.

Current and force data were collected every 34 ms over 70 s while varying forces were applied. Net charge transfer was calculated by numerically integrating the current signal (rectangle method). Example current, charge (with linear baseline correction), and force data are shown in Appendix Figure 10.
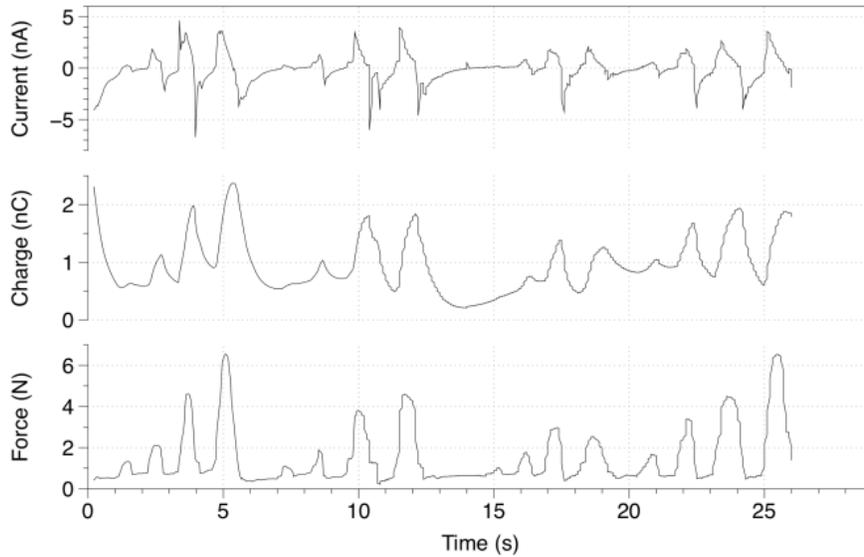
Appendix Figure 10. Measured current, charge (integrated current), and measured force over time during sample testing.

Figure 6.2 plots peak heights from the charge signal against peak heights from the force signal in Appendix Figure 10. Error bars are from the specified force sensor accuracy (5%) and sourcemeter current accuracy multiplied by 1 second (18 pC). The charge is proportional to the force until a saturation point, apparently corresponding to compression of the foam to ~20 – 30% of its original thickness. Regression over the linear region gives the d_{33} piezocoefficient in pC N^{-1} with error bars from the fit. In cases where several measurements were made of the same condition (Figure 6.2), error bars were the standard error across multiple samples.

This measurement setup was validated using commercial PVDF samples, which were measured to have piezocoefficients of 27.3 ± 4.0 pC/N, consistent with the reported value.

A.3   USE OF ACETONE AS DOPANT SOLVENT
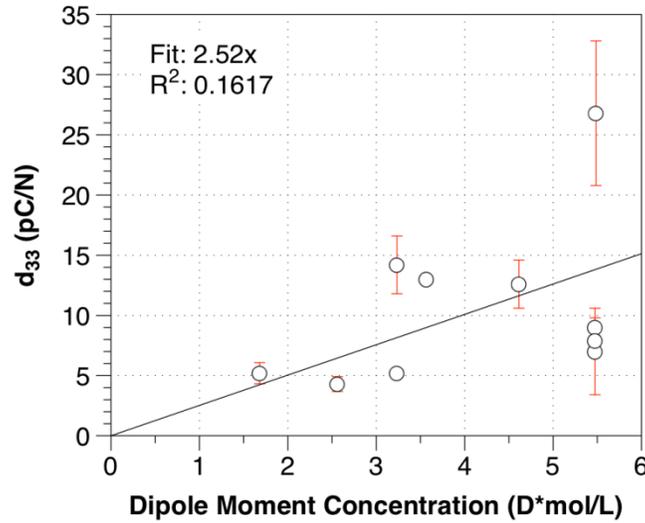
Appendix Figure 11. Piezocoefficient as a function of dipole moment concentration for samples prepared with added acetone.

Higher dopant concentrations were obtained with the addition of acetone. Although these data in Appendix Figure 11 also show a positive correlation between piezocoefficient and dipole moment concentration, it is a much weaker correlation ($R^2 = 0.161$) and with a lower slope than without acetone, plotted in Figure 6.1.

A.4   EFFECT OF HUMIDITY

It was also observed that increased ambient humidity had a negative influence on the piezocoefficient. Less than 10% of doped samples poled in lab conditions of relative humidity of 35 – 40% had responses distinguishable from control, in comparison to over 90% poled in

relatively humidity of 20 – 25%. During periods of ambient humidity over 40%, precursors were mixed and poled in a glove bag with nitrogen fill (RH < 22%) and measured and stored in ambient conditions, leading to a yield of over 70%. Although the specific source of this influence is unknown, it may also be related to the reduction of response with added acetone. Glovebag samples showed somewhat higher responses than samples prepared in dry ambient conditions but follow the same trends.

A.5   STABILITY
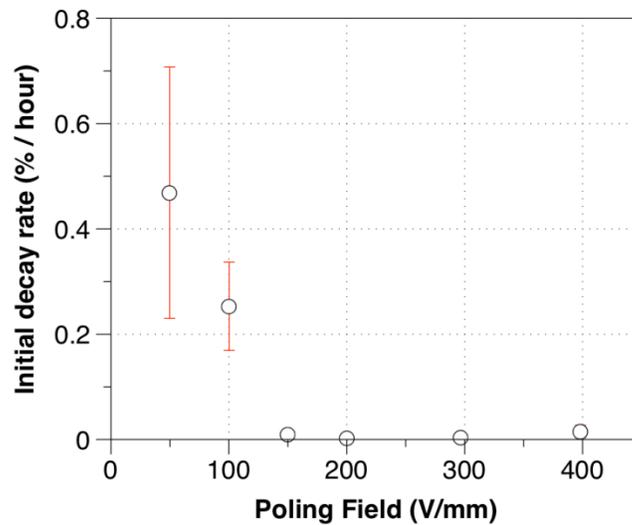
Appendix Figure 12. Initial decay rate of piezoresponse as a function of poling field.

A.6   CHLORONITROANILINE STRUCTURE

CNA crystallizes in a centrosymmetric structure, as shown below:
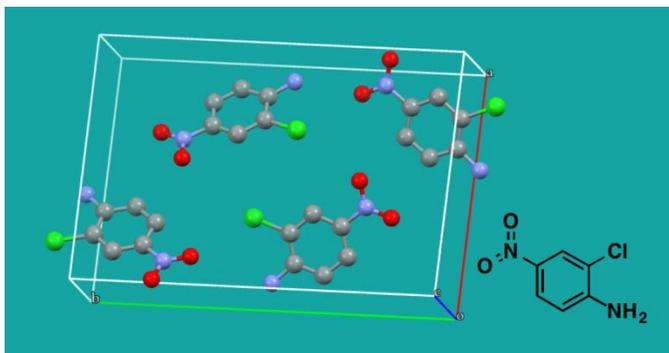
Appendix Figure 13. The crystal structure of 2-chloro-4-nitroaniline. (Structure data from [116]) Note that the unit cell is centrosymmetric.

A.7 ϵ_∞ CALCULATION

As ϵ_∞ represents the dielectric response in the absence of permanent dipole motion, it cannot be experimentally measured under quasistatic conditions. It can however, be estimated from the Clausius-Mossotti equation given in Equation S1.

$$\frac{\epsilon_\infty - 1}{\epsilon_\infty + 2} \epsilon_0 V_m = \frac{4\pi}{3} N\alpha \tag{S1}$$

where V_m is the molar volume, N is Avogadro's number, and α is the molecular polarizability.

For the case of benzoic acid ($\alpha \approx 2 \times 10^{-39}$ C^2 m^2 J^{-1}) [S3] at a concentration of 1 M, ϵ_∞ works out to be 5.0. A dielectric constant of 4 corresponds to a doubling of polarization with the factor of Equation S2 and appears to be within the range of realistic materials.

$$\frac{\epsilon_\infty + 2}{3} \tag{S2}$$

A.8   FOAM VOID DIMENSION MEASUREMENTS
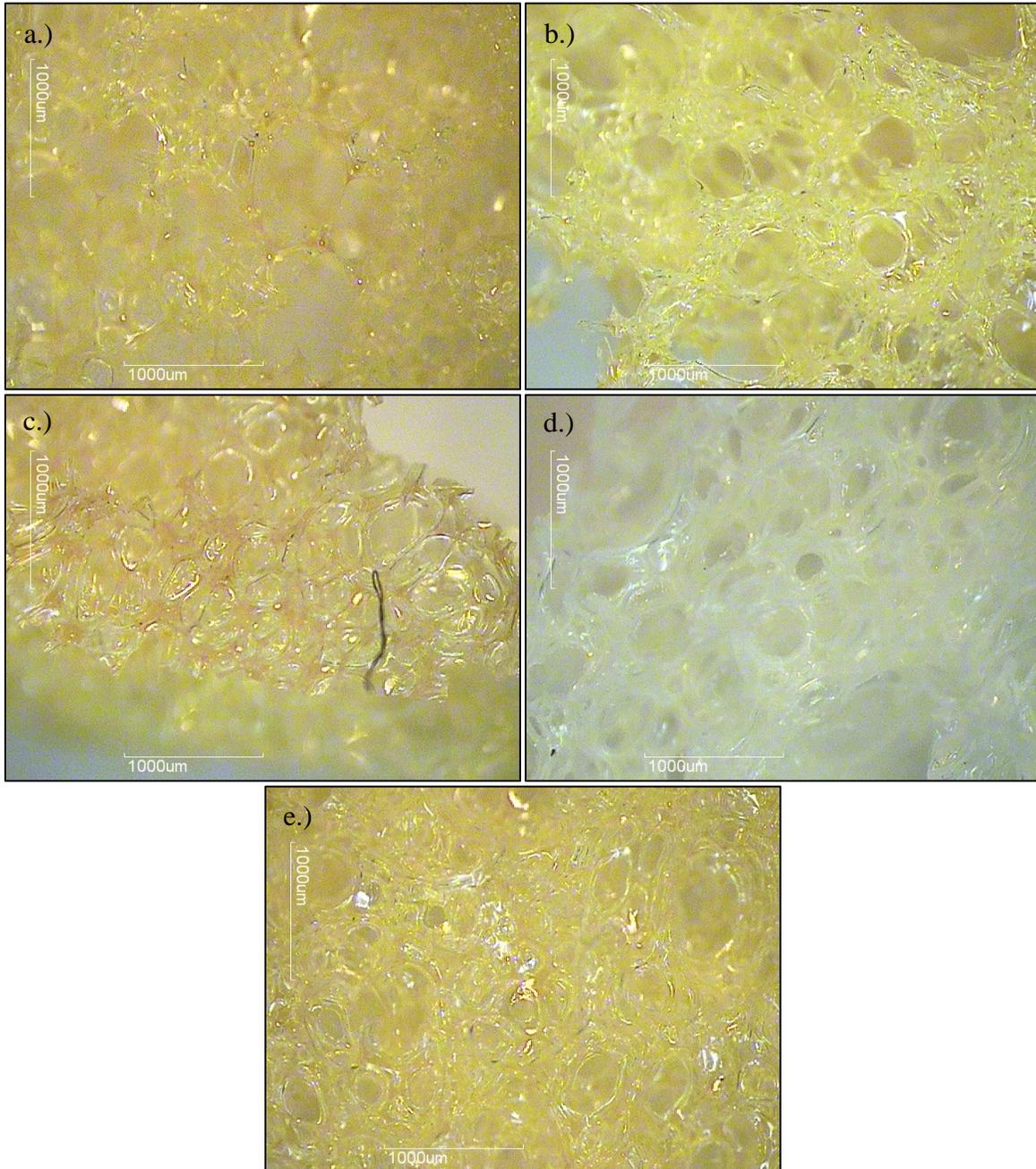
Appendix Figure 14. Micrographs of a.) non-poled sample, b.) 150 V, c.) 500 V, d.) 1051 V, and 2000 V poled samples.
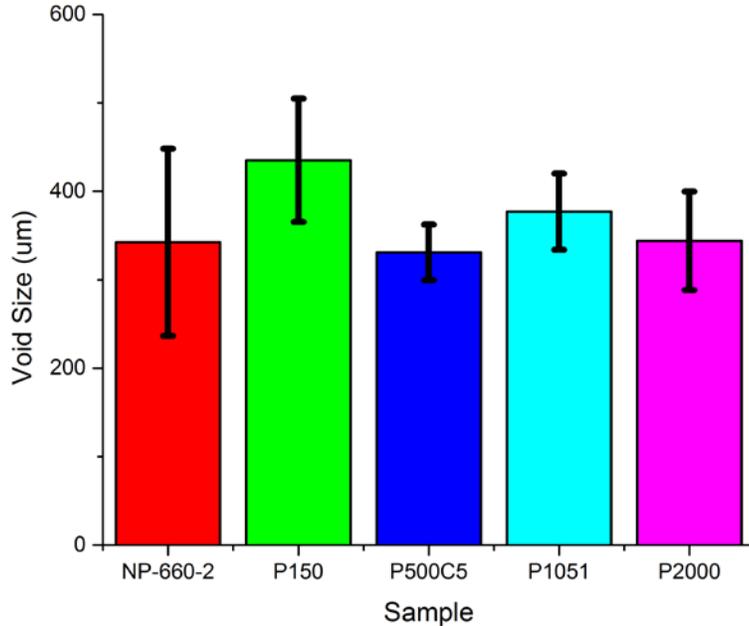
Appendix Figure 15. Average void size with error of samples above. NP – non-poled and P is poled.

A.9   OTHER TESTING METHODS

In principle, it would also be possible to measure the converse piezoelectric effect mechanically. This would, however, be experimentally challenge. For an applied voltage up to 200 V, the deformation from a material with d_{33} = 250 pC N^{-1} would be 50 nm. For a sample with a cross section of 1 cm^2 and a thickness of 5 mm, the effective spring constant would be 11 kN m^{-1} and the force for this deformation would be 0.56 mN. Such deflections would be better measured by laser interferometry.

BIBLIOGRAPHY

1. Dagdeviren, C.; Yang, B. D.; Su, Y.; Tran, P. L.; Joe, P.; Anderson, E.; Xia, J.; Doraiswamy, V.; Dehdashti, B.; Feng, X.; Lu, B.; Poston, R.; Khalpey, Z.; Ghaffari, R.; Huang, Y.; Slepian, M. J.; Rogers, J. A., *Proc. Natl. Acad. Sci.* **2014,** *111* (5), 1927-1932.

2. Akaydin, H. D.; Elvin, N.; Andreopoulos, Y., *J. Intell. Mater. Syst. Struct.* **2010,** *21* (13), 1263-1278.

3. Ottman, G. K.; Hofmann, H. F.; Bhatt, A. C.; Lesieutre, G. A., *IEEE Transactions on Power Electronics* **2002,** *17* (5), 669-676.

4. Dosch, J. J.; Inman, D. J.; Garcia, E., *J. Intell. Mater. Syst. Struct.* **1992,** *3* (1), 166-185.

5. Taylor, S. G.; Raby, E. Y.; Farinholt, K. M.; Park, G.; Todd, M. D., *Struct. Health Monit.* **2016**, 1475921716642171.

6. Demidov, B.; Efremov, V.; Kazakov, E.; Kalinin, Y. G.; Metelkin, S. Y.; Potapenko, A.; Petrov, V., *Instrum. Exp. Tech.* **2016,** *59* (2), 258-261.

7. Zhoujian, L.; Willoquet, G.; Guillot, G.; Hosseinnezhadian, S.; Jourdain, L.; Poirier-quinot, M.; Darrasse, L.; Ginefri, J.-C., *Sens. Actuators, A* **2016,** *241*, 176-189.

8. Shafik, A.; Mrad, R. B., Piezoelectric Motor Technology: A Review. In *Nanopositioning Technologies*, Springer: 2016; pp 33-59.

9. Zandesh, G.; Gheibi, A.; Bafqi, M. S.; Bagherzadeh, R.; Ghoorchian, M.; Latifi, M., *J. Ind. Text.* **2016**, 1528083716647201.

10. Adhikari, S.; Friswell, M.; Litak, G.; Khodaparast, H. H., *Smart Mater. Struct.* **2016,** *25* (6), 65009-65024.

11. Muralt, P.; Marzencki, M.; Belgacem, B.; Calame, F.; Basrour, S., *Procedia Chem.* **2009,** *1* (1), 1191-1194.

12. Wang, Z. L.; Song, J., *Science* **2006,** *312* (5771), 242.

13. Chure, M.-C.; Wu, L.; Wu, K.-K.; Tung, C.-C.; Lin, J.-S.; Ma, W.-C., *Ceram. Int.* **2014,** *40* (1, Part A), 341-345.

14.   Liao, Q.; Zhang, Z.; Zhang, X.; Mohr, M.; Zhang, Y.; Fecht, H.-J., *Nano Res.* **2014,** *7* (6), 917-928.

15.   Mengdi, H.; Yi Chiang, C.; Wen, L.; Shouhe, Z.; Haixia, Z. In *Low frequency PVDF piezoelectric energy harvester with combined d31 and d33 operating modes*, The 8th Annual IEEE International Conference on Nano/Micro Engineered and Molecular Systems, 7-10 April 2013; 2013; pp 440-443.

16.   Jaffe, B., *Piezoelectric ceramics*. Elsevier: 2012; Vol. 3.

17.   Nye, J. F., *Physical properties of crystals: their representation by tensors and matrices*. Oxford university press: 1985.

18.   Newcastle University Piezoelectric Crystal Classes. https://www.staff.ncl.ac.uk/j.p.goss/symmetry/PP_Piezo.html (accessed 24 May 2016).

19.   Birkholz, M., *Zeitschrift fur Physik B: Condensed Matter* **1995,** *96* (3), 333-340.

20.   Kueppers, H.; Leuerer, T.; Schnakenberg, U.; Mokwa, W.; Hoffmann, M.; Schneller, T.; Boettger, U.; Waser, R., *Sens. Actuators, A* **2002,** *97*, 680-684.

21.   Choi, M. Y.; Choi, D.; Jin, M. J.; Kim, I.; Kim, S. H.; Choi, J. Y.; Lee, S. Y.; Kim, J. M.; Kim, S. W., *Adv. Mater.* **2009,** *21* (21), 2185-2189.

22.   Bechmann, R., *Phys. Rev.* **1958,** *110* (5), 1060.

23.   Wang, H.; Zhang, Q.; Cross, L.; Sykes, A., *J. Appl. Phys.* **1993,** *74* (5), 3394-3398.

24.   Zhu, H.; Wang, Y.; Xiao, J.; Liu, M.; Xiong, S.; Wong, Z. J.; Ye, Z.; Yin, X.; Zhang, X., *arXiv preprint arXiv:1408.7074* **2014**.

25.   Werling, K. A.; Hutchison, G. R.; Lambrecht, D. S., *J. Phys. Chem. Lett.* **2013,** *4* (9), 1365-1370.

26.   Love, J. C.; Estroff, L. A.; Kriebel, J. K.; Nuzzo, R. G.; Whitesides, G. M., *Chem. Rev.* **2005,** *105* (4), 1103-1170.

27.   Poirier, G. E.; Pylant, E. D., *Science* **1996,** *272* (5265), 1145.

28.   Laibinis, P. E.; Whitesides, G. M.; Allara, D. L.; Tao, Y. T.; Parikh, A. N.; Nuzzo, R. G., *J. Am. Chem. Soc.* **1991,** *113* (19), 7152-7167.

29.   Love, J. C.; Wolfe, D. B.; Haasch, R.; Chabinyc, M. L.; Paul, K. E.; Whitesides, G. M.; Nuzzo, R. G., *J. Am. Chem. Soc.* **2003,** *125* (9), 2597-2609.

30.   Li, Z.; Chang, S.-C.; Williams, R. S., *Langmuir* **2003,** *19* (17), 6744-6749.

31.   Kalinin, S. V.; Bonnell, D. A., *Phys. Rev. B* **2002,** *65* (12), 125408.

32.   Güthner, P.; Dransfeld, K., *Appl. Phys. Lett.* **1992,** *61* (9), 1137-1139.

33.   Alexe, M.; Gruverman, A., *Nanoscale Characterisation of Ferroelectric Materials: Scanning Probe Microscopy Approach*. Springer Berlin Heidelberg: 2013.

34.   Jungk, T.; Hoffmann, Á.; Soergel, E., *Appl. Phys. Lett.* **2006,** *89* (16), 163507.

35.   Brian, J. R.; Clint, C.; Sergei, V. K.; Roger, P., *Nanotechnology* **2007,** *18* (47), 475504.

36.   Jungk, T.; Hoffmann, Á.; Soergel, E., *Appl. Phys. A* **2007,** *86* (3), 353-355.

37.   Jalalian, A.; Grishin, A. M., *Appl. Phys. Lett.* **2014,** *104* (24), 243701.

38.   Frisch, M. J.; Trucks, G. W.; Schlegel, H. B.; Scuseria, G. E.; Robb, M. A.; Cheeseman, J. R.; Scalmani, G.; Barone, V.; Mennucci, B.; Petersson, G. A.; Nakatsuji, H.; Caricato, M.; Li, X.; Hratchian, H. P.; Izmaylov, A. F.; Bloino, J.; Zheng, G.; Sonnenberg, J. L.; Hada, M.; Ehara, M.; Toyota, K.; Fukuda, R.; Hasegawa, J.; Ishida, M.; Nakajima, T.; Honda, Y.; Kitao, O.; Nakai, H.; Vreven, T.; Montgomery Jr., J. A.; Peralta, J. E.; Ogliaro, F.; Bearpark, M. J.; Heyd, J.; Brothers, E. N.; Kudin, K. N.; Staroverov, V. N.; Kobayashi, R.; Normand, J.; Raghavachari, K.; Rendell, A. P.; Burant, J. C.; Iyengar, S. S.; Tomasi, J.; Cossi, M.; Rega, N.; Millam, N. J.; Klene, M.; Knox, J. E.; Cross, J. B.; Bakken, V.; Adamo, C.; Jaramillo, J.; Gomperts, R.; Stratmann, R. E.; Yazyev, O.; Austin, A. J.; Cammi, R.; Pomelli, C.; Ochterski, J. W.; Martin, R. L.; Morokuma, K.; Zakrzewski, V. G.; Voth, G. A.; Salvador, P.; Dannenberg, J. J.; Dapprich, S.; Daniels, A. D.; Farkas, Ö.; Foresman, J. B.; Ortiz, J. V.; Cioslowski, J.; Fox, D. J. *Gaussian 09*, Gaussian, Inc.: Wallingford, CT, USA, 2009.

39.   Becke, A. D., *J. Chem. Phys.* **1993,** *98* (7), 5648.

40.   Grimme, S.; Antony, J.; Ehrlich, S.; Krieg, H., *J. Chem. Phys.* **2010,** *132* (15), 154104.

41.   Swart, M.; Solà, M.; Bickelhaupt, F. M., *J. Comput. Chem.* **2011,** *32* (6), 1117-1127.

42.   Ehrlich, S.; Moellmann, J.; Grimme, S., *Acc. Chem. Res.* **2013,** *46* (4), 916-926.

43.   Grimme, S., *J. Comput. Chem.* **2006,** *27* (15), 1787-1799.

44.   Yanai, T.; Tew, D. P.; Handy, N. C., *Chem. Phys. Lett.* **2004,** *393* (1–3), 51-57.

45.   Adamo, C.; Barone, V., *J. Chem. Phys.* **1999,** *110* (13), 6158-6170.

46.   Chai, J.-D.; Head-Gordon, M., *J. Chem. Phys.* **2008,** *128* (8), 084106.

47.   Hanwell, M. D.; Curtis, D. E.; Lonie, D. C.; Vandermeersch, T.; Zurek, E.; Hutchison, G., *J. Cheminf.* **2012,** *4* (1), 17.

48.   Lent, C. S.; Isaksen, B.; Lieberman, M., *J. Am. Chem. Soc.* **2003,** *125* (4), 1056-63.

49.   Nilsson, D.; Chen, M. X.; Kugler, T.; Remonen, T.; Armgarth, M.; Berggren, M., *Adv. Mater.* **2002,** *14* (1), 51-54.

50.   Kitagawa, K.; Morita, T.; Kimura, S., *Angew. Chem. Int. Ed.* **2005,** *44* (39), 6330-6333.

51.   Uchino, K., *Ferroelectric Devices*. Marcel Dekker: New York, 2000; p x, 308 p.

52.   Nalwa, H. S., *Handbook of Low and High Dielectric Constant Materials and Their Applications*. Academic Press: San Diego, 1999.

53.   Wang, X.; Zhou, J.; Song, J.; Liu, J.; Xu, N.; Wang, Z. L., *Nano Lett.* **2006,** *6* (12), 2768-72.

54.   Chang, C.; Tran, V. H.; Wang, J.; Fuh, Y. K.; Lin, L., *Nano Lett.* **2010,** *10* (2), 726-31.

55.   Park, K.-I.; Xu, S.; Liu, Y.; Hwang, G.-T.; Kang, S.-J. L.; Wang, Z. L.; Lee, K. J., *Nano Lett.* **2010,** *10* (12), 4939-4943.

56.   Galassi, C., *Piezoelectric Materials : Advances in Science, Technology, and Applications*. Kluwer Academic Publishers: Dordrecht ; Boston, 2000; p xiii, 405 p.

57.   Manalis, S. R.; Minne, S. C.; Quate, C. F., *Appl. Phys. Lett.* **1996,** *68* (6), 871-873.

58.   Indermuhle, P. F.; Schurmann, G.; Racine, G. A.; deRooij, N. F., *J Micromech Microeng* **1997,** *7* (3), 218-220.

59.   Shirane, G.; Hoshino, S.; Suzuki, K., *Phys. Rev.* **1950,** *80* (6), 1105-1106.

60.   Zhang, Q. M.; Bharti, V.; Zhao, X., *Science* **1998,** *280* (5372), 2101-2104.

61.   Simpson, J. O.; Welch, S. S.; St. Clair, T. L., *Mater. Res. Soc. Symp. Proc.* **1996,** *413*, 351.

62.   Qin, Y.; Wang, X. D.; Wang, Z. L., *Nature* **2008,** *451* (7180), 809-U5.

63.   Song, J. H.; Wang, X. D.; Liu, J.; Liu, H. B.; Li, Y. L.; Wang, Z. L., *Nano Lett.* **2008,** *8* (1), 203-207.

64.   Zhu, G.; Wang, A. C.; Liu, Y.; Zhou, Y.; Wang, Z. L., *Nano Lett.* **2012,** *12* (6), 3086-90.

65.   Birkholz, M., *Z. Phys. B: Condens. Matter* **1995,** *96* (3), 325-332.

66.   Murayama, N.; Nakamura, K.; Obara, H.; Segawa, M., *Ultrasonics* **1976,** *14* (1), 15-24.

67.   Clays, K.; Wostyn, K.; Persoons, A.; Stefano, M. B.; Maiorana, S.; Papagni, A.; Daul, C. A.; Weber, V., *Chem. Phys. Lett.* **2003,** *372* (3-4), 438-442.

68.   Feringa, B. L.; Huck, N. P. M.; Schoevaars, A. M., *Adv. Mater.* **1996,** *8* (8), 681-&.

69.   Kelly, T. R.; Cai, X.; Damkaci, F.; Panicker, S. B.; Tu, B.; Bushell, S. M.; Cornella, I.; Piggott, M. J.; Salives, R.; Cavero, M.; Zhao, Y.; Jasmin, S., *J. Am. Chem. Soc.* **2007,** *129* (2), 376-86.

70.   Kim, C.; Marks, T. J.; Facchetti, A.; Schiavo, M.; Bossi, A.; Maiorana, S.; Licandro, E.; Todescato, F.; Toffanin, S.; Muccini, M.; Graiff, C.; Tiripicchio, A., *Org. Electron.* **2009,** *10* (8), 1511-1520.

71.   Zhao, M. H.; Wang, Z. L.; Mao, S. X., *Nano Lett.* **2004,** *4* (4), 587-590.

72.   Chen, Y. Q.; Zheng, X. J.; Feng, X., *Nanotechnology* **2010,** *21* (5), 055708.

73.   Hammett, L. P., *J. Am. Chem. Soc* **1937,** *59* (1), 96-103.

74.   Hansch, C.; Leo, A.; Taft, R. W., *Chem. Rev.* **1991,** *91* (2), 165-195.

75.   Tuukkanen, S.; Julin, T.; Rantanen, V.; Zakrzewski, M.; Moilanen, P.; Lupo, D., *Jpn. J. Appl. Phys.* **2013,** *52* (5S1), 05DA06.

76.   Trotta, R.; Atkinson, P.; Plumhof, J. D.; Zallo, E.; Rezaev, R. O.; Kumar, S.; Baunack, S.; Schroter, J. R.; Rastelli, A.; Schmidt, O. G., *Adv. Mater.* **2012,** *24* (20), 2668-72.

77.   Fan, F. R.; Tang, W.; Wang, Z. L., *Adv. Mater.* **2016**.

78.   Park, K. I.; Son, J. H.; Hwang, G. T.; Jeong, C. K.; Ryu, J.; Koo, M.; Choi, I.; Lee, S. H.; Byun, M.; Wang, Z. L.; Lee, K. J., *Adv. Mater.* **2014,** *26* (16), 2514-20.

79.   Bystrov, V. S.; Paramonova, E. V.; Bdikin, I. K.; Bystrova, A. V.; Pullar, R. C.; Kholkin, A. L., *J. Mol. Model.* **2013,** *19* (9), 3591-602.

80.   Moody, M. J.; Marvin, C. W.; Hutchison, G. R., *Journal of Materials Chemistry C* **2016,** *4* (20), 4387-4392.

81.   Quan, X.; Marvin, C. W.; Seebald, L.; Hutchison, G. R., *J. Phys. Chem. C* **2013,** *117* (33), 16783-16790.

82.   Jackson, M.; Mantsch, H. H., *Crit. Rev. Biochem. Mol. Biol.* **1995,** *30* (2), 95-120.

83. Yang, H.; Yang, S.; Kong, J.; Dong, A.; Yu, S., *Nat. Protocols* **2015,** *10* (3), 382-396.

84. Lu, H.; Hood, M. A.; Mauri, S.; Baio, J. E.; Bonn, M.; Munoz-Espi, R.; Weidner, T., *Chem. Commun.* **2015,** *51* (88), 15902-15905.

85. Carr, P. H., *Journal of the Acoustical Society of America* **1967,** *41* (1), 75-83.

86. Eiichi, F.; Iwao, Y., *Jpn. J. Appl. Phys.* **1964,** *3* (2), 117.

87. Marino, A. A.; Becker, R. O.; Soderholm, S. C., *Calcified Tissue Research* **1971,** *8* (1), 177-180.

88. Eiichi, F., *J. Phys. Soc. Jpn.* **1955,** *10* (2), 149-154.

89. Guichard, G.; Huc, I., *Chem. Commun.* **2011,** *47* (21), 5933-5941.

90. Kim, K.; Zhu, W.; Qu, X.; Aaronson, C.; McCall, W. R.; Chen, S.; Sirbuly, D. J., *ACS Nano* **2014,** *8* (10), 9799-9806.

91. Park, K. I.; Lee, M.; Liu, Y.; Moon, S.; Hwang, G. T.; Zhu, G.; Kim, J. E.; Kim, S. O.; Kim, D. K.; Wang, Z. L.; Lee, K. J., *Adv. Mater.* **2012,** *24*, 2999.

92. Jana, S.; Garain, S.; Sen, S.; Mandal, D., *PCCP* **2015,** *17* (26), 17429-17436.

93. Gerhard-Multhaupt, R., *IEEE Trans. Dielectr. Electr. Insul.* **2002,** *9* (5), 850-859.

94. Wang, F.; Mai, Y.-W.; Wang, D.; Ding, R.; Shi, W., *Sens. Actuators, A* **2015,** *233*, 195-201.

95. Qi, Y.; Jafferis, N. T.; Lyons, K.; Lee, C. M.; Ahmad, H.; McAlpine, M. C., *Nano Lett.* **2010,** *10* (2), 524-528.

96. Bowen, C. R.; Kim, H. A.; Weaver, P. M.; Dunn, S., *Energy Environ. Sci.* **2014,** *7* (1), 25-44.

97. Sam, C.; Sohini, K.-N., *Nanotechnology* **2015,** *26* (34), 344001.

98. Cardoso, V. F.; Costa, C. M.; Minas, G.; Lanceros-Mendez, S., *Smart Mater. Struct.* **2012,** *21* (8), 085020.

99. Hillenbrand, J.; Sessler, G. M., *IEEE Trans. Dielectr. Electr. Insul.* **2004,** *11* (1), 72-79.

100. Anton, S. R.; Farinholt, K. M.; Erturk, A., *J. Intell. Mater. Syst. Struct.* **2014,** *25* (14), 1681-1692.

101. Paajanen, M.; Wegener, M.; Gerhard-Multhaupt, R., *J. Phys. D: Appl. Phys.* **2001,** *34* (16), 2482.

102. Khaled, S. R.; Sameoto, D.; Evoy, S., *Smart Mater. Struct.* **2014,** *23* (3), 033001.

103. Shi, Y.; Zhang, C.; Zhang, H.; Bechtel, J. H.; Dalton, L. R.; Robinson, B. H.; Steier, W. H., *Science* **2000,** *288* (5463), 119.

104. Ma, H.; Liu, S.; Luo, J.; Suresh, S.; Liu, L.; Kang, S. H.; Haller, M.; Sassa, T.; Dalton, L. R.; Jen, A. K. Y., *Adv. Funct. Mater.* **2002,** *12* (9), 565-574.

105. Min-Cheol, O.; Hua, Z.; Cheng, Z.; Erlig, H.; Yian, C.; Tsap, B.; Chang, D.; Szep, A.; Steier, W. H.; Fetterman, H. R.; Dalton, L. R., *IEEE. J. Sel. Top. Quantum Electron.* **2001,** *7* (5), 826-835.

106. Lee, J.-Y.; Jin, M.-K.; Park, E.-J., *Polym. Bull.* **2000,** *45* (1), 17-23.

107. Burland, D. M.; Miller, R. D.; Walsh, C. A., *Chem. Rev.* **1994,** *94* (1), 31-75.

108. Mopsik, F. I.; Broadhurst, M. G., *J. Appl. Phys.* **1975,** *46* (10), 4204-4208.

109. Balakina, M. Y., *J. Non-Cryst. Solids* **2007,** *353* (47–51), 4432-4436.

110. Kono, R., *J. Phys. Soc. Jpn.* **1960,** *15* (4), 718-725.

111. Sborikas, M.; Wegener, M., *Appl. Phys. Lett.* **2013,** *103* (25), 252901.

112. Mao, Y.; Zhao, P.; McConohy, G.; Yang, H.; Tong, Y.; Wang, X., *Adv. Energy Mater.* **2014,** *4* (7), 1301624-n/a.

113. Cha, S.; Kim, S. M.; Kim, H.; Ku, J.; Sohn, J. I.; Park, Y. J.; Song, B. G.; Jung, M. H.; Lee, E. K.; Choi, B. L.; Park, J. J.; Wang, Z. L.; Kim, J. M.; Kim, K., *Nano Lett.* **2011,** *11* (12), 5142-5147.

114. Zhu, H. X.; Knott, J. F.; Mills, N. J., *J. Mech. Phys. Solids* **1997,** *45* (3), 319-343.

115. Aloui, F.; El Abed, R.; Marinetti, A.; Ben Hassine, B., *Tetrahedron Lett.* **2007,** *48* (11), 2017-2020.

116. McPhail, A. T.; Sim, G. A., *J. Chem. Soc.* **1965,** (0), 227-236.